that were eventually incorporated into the thrombi (data not shown), causes us to speculate that the role of tissue factor may not have been important in the initiation of the activation of the coagulation cascade around the platelet thrombi, at least in our flow chamber system. Nevertheless, some investigators have demonstrated the initiation of the coagulation cascade by phospholipids and Factor XI on erythrocytes, even in the absence of tissue factor,[49] which may be relevant to our present results. In any case, further investigations are required to elucidate the correct mechanism of the initiation of the activation of the coagulation cascade on the surface of the platelet thrombi under blood flow conditions.

In conclusion, in experiments using human blood under artificial blood flow conditions, we have demonstrated, using a 2-color imaging system, the local production of fibrin around the surface of activated platelets (activated platelet-derived procoagulant activity) forming thrombi, even in the presence of specific antithrombin agents in the blood in amounts sufficient to maintain the fluidity of the blood during the experiments. We have shown a positive relationship between the magnitude of the increase in the $[Ca^{2+}]_i$ of the platelets incorporated within thrombi and the amount of fibrin monomer complex generated around them. We have also demonstrated the role of increased $[Ca^{2+}]_i$ of the platelets incorporated within the thrombi in maintaining the stability of the platelet thrombi and, consequently, their 3-D growth. The recognition of these functional links between the activation of the platelets and local activation of the coagulation cascade around them may provide new insight into the crucial role of platelet-derived procoagulant activity in the regulation of arterial thrombus growth. Our results suggest a regulatory role of both the activation of the coagulation cascade on the surface of platelet thrombi and the local generation of thrombin, even under arterial blood flow conditions, not only in the local generation of fibrin fibrils around platelet thrombi but also in maintaining the stability of platelet thrombi and further enhancing procoagulant activity related to the activation of phospholipid scramblase following an increase in the $[Ca^{2+}]_i$ of the platelets forming thrombi. We have thus shown a close functional linkage between the activation of platelets and the coagulation system even under arterial blood flow conditions.

## Acknowledgments

We gratefully acknowledge the contribution of the staff of Tokai University Educational and Research Support Center. This work was supported in part by a Grant-in-Aid for Scientific Research in Japan (15590771, 17590764, 19590871), Tokai University School of Medicine, Project Research 2006, a grant from the Vehicle Racing Commemorative Foundation, a grant for the Leading Project and Next Generation of the Integrated Biological Simulator Developing Program Supported by the Ministry of Education and Science, Sports and Culture, Japan, and a grant for the next-generation supercomputer Research and Development program supported by RIKEN, and a grant for Regulatory Medicine supported by the Ministry of Health, Labor and Welfare, Japan, to S.G.

## References

1. Ruggeri ZM. Platelets in atherothrombosis. *Nat Med* 2002; **8:** 1227–1234.
2. Hoshiba Y, Hatakeyama K, Tanabe T, Asada Y, Goto S. Co-localization of von Willebrand factor with platelet thrombi, tissue factor and platelets with fibrin, and consistent presence of inflammatory cells in coronary thrombi obtained by an aspiration device from patients with acute myocardial infarction. *J Thromb Haemost* 2006; **4:** 114–120.
3. Yamashita A, Sumi T, Goto S, Hoshiba Y, Nishihira K, Kawamoto R, et al. Detection of von Willebrand factor and tissue factor in platelets-fibrin rich coronary thrombi in acute myocardial infarction. *Am J Cardiol* 2006; **97:** 26–28.
4. Goto S. Understanding the mechanism and prevention of arterial occlusive thrombus formation by anti-platelet agents. *Curr Med Chem Cardiovasc Hematol Agents* 2004; **2:** 149–156.
5. Ma YQ, Qin J, Plow EF. Platelet integrin $\alpha$(IIb) $\beta$: Activation mechanisms. *J Thromb Haemost* 2007; **5:** 1345–1352.
6. Mackman N, Tilley RE, Key NS. Role of the extrinsic pathway of blood coagulation in hemostasis and thrombosis. *Arterioscler Thromb Vasc Biol* 2007; **27:** 1687–1693.
7. Gailani D, Renne T. Intrinsic pathway of coagulation and arterial thrombosis. *Arterioscler Thromb Vasc Biol* 2007; **27:** 2507–2513.
8. Libby P, Aikawa M. Stabilization of atherosclerotic plaques: New mechanisms and clinical targets. *Nat Med* 2002; **8:** 1257–1262.
9. Goto S. Propagation of arterial thrombi: Local and remote contributory factors. *Arterioscler Thromb Vasc Biol* 2004; **24:** 2207–2208.
10. Gawaz M, Langer H, May AE. Platelets in inflammation and atherogenesis. *J Clin Invest* 2005; **115:** 3378–3384.
11. Wagner DD, Burger PC. Platelets in inflammation and thrombosis. *Arterioscler Thromb Vasc Biol* 2003; **23:** 2131–2137.
12. Strukova SM. Role of platelets and serine proteinases in coupling of blood coagulation and inflammation. *Biochemistry (Mosc)* 2004; **69:** 1067–1081.
13. Gear AR, Camerini D. Platelet chemokines and chemokine receptors: Linking hemostasis, inflammation, and host defense. *Microcirculation* 2003; **10:** 335–350.
14. Goto S, Tamura N, Eto K, Ikeda Y, Handa S. Functional significance of adenosine 5'-diphosphate receptor (P2Y(12)) in platelet activation initiated by binding of von Willebrand factor to platelet GP Iba induced by conditions of high shear rate. *Circulation* 2002; **105:** 2531–2536.
15. Dachary-Prigent J, Pasquet JM, Freyssinet JM, Nurden AT. Calcium involvement in aminophospholipid exposure and microparticle formation during platelet activation: A study using $Ca^{2+}$-ATPase inhibitors. *Biochemistry* 1995; **34:** 11625–11634.
16. Tamura N, Yoshida M, Ichikawa N, Handa M, Ikeda Y, Tanabe T, et al. Shear-induced von Willebrand factor-mediated platelet surface translocation of the CD40 ligand. *Thromb Res* 2002; **108:** 311–315.
17. Youssef AA, Chang LT, Sheu JJ, Lee FY, Chua S, Yeh KH, et al. Association between circulating level of CD40 ligand and angiographic morphologic features indicating high-burden thrombus formation in patients with acute myocardial infarction undergoing primary coronary intervention. *Circ J* 2007; **71:** 1857–1861.
18. Henn V, Slupsky JR, Grafe M, Anagnostopoulos I, Forster R, Muller-Berghaus G, et al. CD40 ligand on activated platelets triggers an inflammatory reaction of endothelial cells. *Nature* 1998; **391:** 591–594.
19. Hagihara M, Higuchi A, Tamura N, Ueda Y, Hirabayashi K, Ikeda Y, et al. Platelets, after exposure to a high shear stress, induce IL-10-producing, mature dendritic cells in vitro. *J Immunol* 2004; **172:** 5297–5303.
20. Miyazaki Y, Nomura S, Miyake T, Kagawa H, Kitada C, Taniguchi H, et al. High shear stress can initiate both platelet aggregation and shedding of procoagulant containing microparticles. *Blood* 1996; **88:** 3456–3464.
21. Reininger AJ, Heijnen HF, Schumann H, Specht HM, Schramm W, Ruggeri ZM. Mechanism of platelet adhesion to von Willebrand factor and microparticle formation under high shear stress. *Blood* 2006; **107:** 3537–3545.
22. Dorsam RT, Tuluc M, Kunapuli SP. Role of protease-activated and ADP receptor subtypes in thrombin generation on human platelets. *J Thromb Haemost* 2004; **2:** 804–812.
23. Coughlin SR. Thrombin signalling and protease-activated receptors. *Nature* 2000; **407:** 258–264.
24. Andre P, Prasad KS, Denis CV, He M, Papalia JM, Hynes RO, et al. CD40L stabilizes arterial thrombi by a beta3 integrin-dependent mechanism. *Nat Med* 2002; **8:** 247–252.
25. Goto S, Tamura N, Handa S, Arai M, Kodama K, Takayama H. Involvement of glycoprotein VI in platelet thrombus formation on both collagen and von Willebrand factor surfaces under flow conditions. *Circulation* 2002; **106:** 266–272.
26. Goto S, Tamura N, Ishida H, Ruggeri ZM. Dependence of platelet thrombus stability on sustained glycoprotein IIb/IIIa activation through adenosine 5'-diphosphate receptor stimulation and cyclic calcium signaling. *J Am Coll Cardiol* 2006; **47:** 155–162.
27. Sakakibara M, Goto S, Eto K, Tamura N, Isshiki T, Handa S. Application of ex vivo flow chamber system for assessment of stent thrombosis. *Arterioscler Thromb Vasc Biol* 2002; **22:** 1360–1364.
28. Savage B, Saldivar E, Ruggeri ZM. Initiation of platelet adhesion by arrest onto fibrinogen or translocation on von Willebrand factor. *Cell* 1996; **84:** 289–297.
29. Nesbitt WS, Giuliano S, Kulkarni S, Dopheide SM, Harper IS,

Jackson SP. Intercellular calcium communication regulates platelet aggregation and thrombus growth. *J Cell Biol* 2003; **160:** 1151–1161.
30. Goto S, Tamura N, Ishida H. Ability of anti-glycoprotein IIb/IIIa agents to dissolve platelet thrombi formed on a collagen surface under blood flow conditions. *J Am Coll Cardiol* 2004; **44:** 316–323.
31. Genka C, Ishida H, Ichimori K, Hirota Y, Tanaami T, Nakazawa H. Visualization of biphasic $Ca^{2+}$ diffusion from cytosol to nucleus in contracting adult rat cardiac myocytes with an ultra-fast confocal imaging system. *Cell Calcium* 1999; **25:** 199–208.
32. Hamano A, Tanaka S, Takeda Y, Umeda M, Sakata Y. A novel monoclonal antibody to fibrin monomer and soluble fibrin for the detection of soluble fibrin in plasma. *Clin Chim Acta* 2002; **318:** 25–32.
33. Falati S, Gross P, Merrill-Skoloff G, Furie BC, Furie B. Real-time in vivo imaging of platelets, tissue factor and fibrin during arterial thrombus formation in the mouse. *Nat Med* 2002; **8:** 1175–1181.
34. Merritt JE, McCarthy SA, Davies MP, Moores KE. Use of fluo-3 to measure cytosolic $Ca^{2+}$ in platelets and neutrophils. Loading cells with the dye, calibration of traces, measurements in the presence of plasma, and buffering of cytosolic $Ca^{2+}$. *Biochem J* 1990; **269:** 513–519.
35. Friedman H, Meir S, Rosenberger I, Halevy AH, Kaufman PB, Philosoph-Hadas S. Inhibition of the gravitropic response of snapdragon spikes by the calcium-channel blocker lanthanum chloride. *Plant Physiol* 1998; **118:** 483–492.
36. Zhou Q, Zhao J, Wiedmer T, Sims PJ. Normal hemostasis but defective hematopoietic response to growth factors in mice deficient in phospholipid scramblase 1. *Blood* 2002; **99:** 4030–4038.
37. Zhou Q, Zhao J, Stout JG, Luhm RA, Wiedmer T, Sims PJ. Molecular cloning of human plasma membrane phospholipid scramblase A protein mediating transbilayer movement of plasma membrane phospholipids. *J Biol Chem* 1997; **272:** 18240–18244.
38. Goto S. Understanding the mechanism of platelet thrombus formation under blood flow conditions and the effect of new antiplatelet agents. *Curr Vasc Pharmacol* 2004; **2:** 23–32.
39. Goto S, Salomon DR, Ikeda Y, Ruggeri ZM. Characterization of the unique mechanism mediating the shear-dependent binding of soluble von Willebrand factor to platelets. *J Biol Chem* 1995; **270:** 23352–23361.
40. Vu TK, Hung DT, Wheaton VI, Coughlin SR. Molecular cloning of a functional thrombin receptor reveals a novel proteolytic mechanism of receptor activation. *Cell* 1991; **64:** 1057–1068.
41. Goto S, Tamura N, Li M, Handa M, Ikeda Y, Handa S, et al. Different effects of various anti-GPIIb-IIIa agents on shear-induced platelet activation and expression of procoagulant activity. *J Thromb Haemost* 2003; **1:** 2022–2030.
42. Andersen H, Greenberg DL, Fujikawa K, Xu W, Chung DW, Davie EW. Protease-activated receptor 1 is the primary mediator of thrombin-stimulated platelet procoagulant activity. *Proc Natl Acad Sci USA* 1999; **96:** 11189–11193.
43. Bahou WF, Scudder L, Rubenstein D, Jesty J. A shear-restricted pathway of platelet procoagulant activity is regulated by IQGAP1. *J Biol Chem* 2004; **279:** 22571–22577.
44. Goto S. Factor XIa as a possible new target of antithrombotic therapy. *J Thromb Haemost* 2006; **4:** 1494–1495.
45. Sims PJ, Wiedmer T. Unraveling the mysteries of phospholipid scrambling. *Thromb Haemost* 2001; **86:** 266–275.
46. Keuren JF, Wielders SJ, Ulrichts H, Hackeng T, Heemskerk JW, Deckmyn H, et al. Synergistic effect of thrombin on collagen-induced platelet procoagulant activity is mediated through protease-activated receptor-1. *Arterioscler Thromb Vasc Biol* 2005; **25:** 1499–1505.
47. London FS, Marcinkiewicz M, Walsh PN. PAR-1-stimulated factor IXa binding to a small platelet subpopulation requires a pronounced and sustained increase of cytoplasmic calcium. *Biochemistry* 2006; **45:** 7289–7298.
48. Falati S, Liu Q, Gross P, Merrill-Skoloff G, Chou J, Vandendries E, et al. Accumulation of tissue factor into developing thrombi in vivo is dependent upon microparticle P-selectin glycoprotein ligand 1 and platelet P-selectin. *J Exp Med* 2003; **197:** 1585–1598.
49. Iwata H, Kaibara M. Activation of factor IX by erythrocyte membranes causes intrinsic coagulation. *Blood Coagul Fibrinolysis* 2002; **13:** 489–496.

*Transfusion Medicine*, 2008, **18**, 158–166 doi: 10.1111/j.1365-3148.2008.00860.x

ORIGINAL ARTICLE

# Haemostatic effects of polymerized albumin particles carrying fibrinogen γ-chain dodecapeptide as platelet substitutes in severely thrombocytopenic rabbits

Y. Okamura,*† T. Fujie,* M. Nogawa, ‡ H. Maruyama,§ M. Handa,† Y. Ikeda§ & S. Takeoka*

**Department of Life Science and Medical Bioscience, Graduate School of Advanced Science and Engineering, Waseda University, †Department of Transfusion Medicine & Cell Therapy, School of Medicine, Keio University, ‡Research and Development Department, Central Blood Institute, Japanese Red Cross Society, and §Department of Internal Medicine, School of Medicine, Keio University, Tokyo, Japan*

*Received 25 October 2007; accepted for publication 27 March 2008*

SUMMARY. Our purpose was to produce a platelet substitute that could enhance haemostatic ability using rabbits with severe thrombocytopenia. We have developed polymerized albumin particles (polyAlb) for treatment of bleeding and focused on a dodecapeptide, HHLGGAKQAGDV (H12), as a useful ligand for activated platelet. This sequence occurs only at the carboxy-terminus of the fibrinogen γ-chain (γ 400–411). H12 was conjugated to the surface of polyAlb modified with poly(ethylene glycol) (PEG) chains to produce blood-compatible particles (H12–PEG–polyAlb) that had prolonged blood residence time and enhanced stability *in vitro* and *in vivo*. The H12–PEG–polyAlb was administered intravenously to rabbits with severe thrombocytopenia, and the ear bleeding time was measured in order to evaluate the haemostatic effect. The H12–PEG–polyAlb significantly shortened the ear bleeding time of severely thrombocytopenic rabbits and showed no effect on the inhibition or promotion of endogenous and exogenous coagulation activities. Furthermore, we could assess the haemostatic capacity of the H12–PEG–polyAlb, based on the relationship between transfused platelet count and the bleeding time. The H12–PEG–polyAlb may be a suitable candidate for an alternative to human platelet concentrates infused to treat bleeding in patients with severe thrombocytopenia.

*Key words:* dodecapeptide (H12), ear bleeding time, PEG modification, platelet substitutes, polymerized albumin particles, thrombocytopenic rabbits.

Platelet transfusion plays an important role in supportive therapy for patients with thrombocytopenia caused by haematological malignancies or resulting from intensive chemotherapy or radiotherapy for cancer. However, the limited supply of platelet concentrates has always been a serious issue because of their short storage life (3 days in Japan), an insufficient number of donations and hence the demand that exceeds the supply. Furthermore, the risk of viral or bacterial infection associated with transfusion is also a serious issue. For these reasons, a number of trials have been conducted to develop platelet substitutes (artificial platelets) that can reproduce platelet functions, such as infusible platelet membranes (Graham *et al.*, 2001), solubilized platelet membrane protein-conjugated liposomes (plateletsomes) (Rybak & Renzulli, 1993), fibrinogen-bonded red blood cells (Agam & Livine, 1992), liposomes bearing fibrinogen (Casals *et al.*, 2003), fibrinogen-coated albumin microcapsules (Synthocytes) (Levi *et al.*, 1999) and arginyl-glycyl-aspartate (RGD) peptide-bound red blood cells (thromboerythrocytes) (Coller *et al.*, 1992). These platelet substitutes consist of materials derived from blood components.

The glycoprotein (GP) IIb/IIIa receptor on the platelet membrane is converted from an inactive to an active form when platelets adhere to collagen at the site of vascular injury (Takagi *et al.*, 2002; Xiao *et al.*, 2004). The activated GPIIb/IIIa acts as a receptor for fibrinogen and von Willebrand factor (Mustard *et al.*, 1978; Ruggeri *et al.*, 1983), and their binding is followed by platelet aggregation (De Marco *et al.*, 1986). This is because fibrinogen contains three putative binding sites for GPIIb/IIIa, namely a tetrapeptide containing an

Correspondence: Shinji Takeoka, 2-2 Wakamatsucho, Shinjuku, Tokyo, 162-8480, Japan.
Tel.: +813 5369 7324; fax: +813 5369 7324;
e-mail: takeoka@waseda.jp

RGD sequence, for example RGDF and RGDS at α 95–98 and α 572–575, respectively, and a dodecapeptide (HHLGGAKQAGDV, H12) at the γ-chain carboxy-terminal sequence (γ 400–411) (Kloczewiak *et al.*, 1982).

In order to construct platelet substitutes having the desired haemostatic effects, we have also conjugated fibrinogen (Takeoka *et al.*, 2001), recombinant platelet membrane GPIbα (Kitaguchi *et al.*, 1999; Takeoka *et al.*, 2000; Nishiya *et al.*, 2002; Takeoka *et al.*, 2002) and GPIa/IIa (Teramura *et al.*, 2003) to biocompatible and biodegradable carriers such as polymerized albumin particles (polyAlb) and phospholipid vesicles (liposomes). In particular, the fibrinogen conjugates were shown to facilitate platelet aggregation *in vitro* on an activated platelet-immobilized surface by recruiting flowing platelets into aggregates after their initial attachment (Takeoka *et al.*, 2001). However, the isolated human fibrinogen protein is not stable (Takeoka *et al.*, 2001) and tends to precipitate at 4 °C within a few hours (Wertheimer *et al.*, 1944).

Therefore, we focused on the H12 sequence instead of full-length fibrinogen (Kloczewiak *et al.*, 1982; Kloczewiak *et al.*, 1984, 1989; Lam *et al.*, 1987). The H12 conjugates showed minimal interaction with non-stimulated platelets compared with RGD conjugates, based on our results obtained from flow cytometric analyses of platelet agglutination (Takeoka *et al.*, 2003; Okamura *et al.*, 2005a). Furthermore, the H12-conjugated polyAlb enhanced the *in vitro* thrombus formation on a collagen surface, and it dose dependently reduced the tail bleeding time of rats with moderate thrombocytopenia (Okamura *et al.*, 2005b). Recently, we succeeded in prolonging the *in vivo* residence time of the H12–polyAlb by poly(ethylene glycol) (PEG) modification (H12–PEG–polyAlb) and confirmed that the H12–PEG–polyAlb haemostatic effects lasted for at least 6 h (Okamura *et al.*, 2007).

Our purpose was to produce a platelet substitute that could enhance haemostatic ability using a larger animal with severe thrombocytopenia (thrombocytopenic rabbits). In this study, the H12–PEG–polyAlb particles were administered intravenously to rabbits, and the ear bleeding time was measured to evaluate the haemostatic effect. Furthermore, we estimated the haemostatic capacity of the H12–PEG–polyAlb based on the relationship between the bleeding time and platelet transfusion.

## MATERIALS AND METHODS

### *Reagents*

Fibrinogen γ-chain dodecapeptide (C-HHLGGAK-QAGDV, H12) was synthesized using a solid-phase synthesizer (BEX, Tokyo, Japan). PEGs, precisely, α-(3-[3-maleimido-1-oxopropyl]amino) propyl-ω-succinimidyl carboxypentyloxy PEG (MALPEG-NHS, molecular weight 5·0 kDa) and α-methoxy-ω-succinimidyl carboxypentyloxy PEG (mPEG-NHS, molecular weight 5·0 kDa), were purchased from NOF (Tokyo, Japan). Busulphan and PEG (average molecular weight, 400 Da) were obtained from Sigma–Aldrich (St. Louis, MO, USA). Recombinant human serum albumin (rHSA) was kindly donated by Mitsubishi Pharma (Osaka, Japan). Ketamine (60 mg $mL^{-1}$) and seractal 2% were purchased from Daiichi-Sankyo (Tokyo, Japan) and Bayer Medical (Tokyo, Japan), respectively. Phycoerythrin-conjugated streptavidin (PE–streptavidin) and *N*-hydroxysuccinimidobiotin (NHS–biotin) were purchased from BD-Pharmingen (San Diego, CA, USA) and Pierce Chemical (Rockford, IL, USA), respectively.

### *Preparation of H12–PEG–polyAlb*

A suspension of polyAlb with an average diameter of 240 ± 100 nm was prepared as described previously (Okamura *et al.*, 2007). A solution of MALPEG-NHS in dimethyl sulfoxide (DMSO) (10 mM, 7·4 mL) was added to the polyAlb suspension (15 mg $mL^{-1}$, 250 mL), and the suspension was stirred for 20 min at room temperature. A solution of mPEG-NHS in DMSO (25 mM, 8·9 mL) was added to the suspension, and the suspension was stirred for 20 min at room temperature. The unreacted reagents and the by-products were separated by repeated centrifugation (30 000 *g*, 20 min, 4 °C, twice) and washed with phosphate-buffered saline (PBS), and MALPEG- and mPEG-modified polyAlb [(MALPEG)(mPEG)polyAlb] were collected. A suspension of (MALPEG)(mPEG)poly-Alb (21 mg $mL^{-1}$, 70 mL) was mixed with a solution of H12 (100 mM, 292 μL) and allowed to react at room temperature for 12 h. A small molar excess of cysteine over MALPEG was added to the suspension, and the unreacted reagents were removed by repeated centrifugation (30 000 *g*, 10 min, 4 °C) and washed with PBS to obtain the purified H12-conjugated (MALPEG) (mPEG)polyAlb (H12–PEG–polyAlb, 30 mg $mL^{-1}$, 15 mL).

The concentrations of MALPEG, mPEG and H12 conjugated to the surface of polyAlb particles were determined by quantifying each unreacted reagent using high-pressure liquid chromatography on a TSK-GEL G3000$PW_{xL}$ column (7·8 mM outer diameter × 300 mm height using a mobile phase of 36% acetonitrile and 0·1% trifluoroacetic acid at 1 mL $min^{-1}$). The unreacted reagents were detected using a reflective index detector.

*Preparation of busulphan-induced thrombocytopenic rabbits*

All animal studies were approved by the Animal Subject Committee of Keio University, School of Medicine, and were performed according to NIH guidelines for the care and use of laboratory animals (NIH publication 85-23 Rev. 1985). Experiments were carried out using male New Zealand white rabbits (approximately 2·5 kg, 11 weeks old; Sankyo Lab, Tokyo, Japan). The rabbits were anaesthetized by intramuscular injection of a 'cocktail' of ketamine (1·5 mL) and seractal 2% (0·5 mL). A busulphan solution was prepared at a concentration of 10 mg $mL^{-1}$ in PEG (average molecular weight, 400 Da). After shaving the hair around the injection sites, the rabbits received a subcutaneous injection of busulphan at a dosage of 15, 20, or 25 mg $kg^{-1}$ on days 0 and 3, to produce a total dosage of 30, 40 or 50 mg $kg^{-1}$, respectively. Blood samples for cell counting were withdrawn from anaesthetized rabbits by inserting a 23-gauge needle into an ear vein, and the cell counts were determined with an automated haematology analyser (K-4500; Sysmex, Kobe, Japan). To maintain adequate anaesthesia, intramuscular injection of ketamine was repeated as the need arose.

*Platelet transfusion*

Blood withdrawn from donor rabbits, which were anaesthetized and then exsanguinated by cardiac puncture, was mixed with a 10% volume of an acid–citrate–dextrose (ACD) solution composed of 2·2% (w/v) sodium citrate, 0·8% (w/v) citric acid and 2·2% (w/v) glucose. Platelet-rich plasma (PRP) was prepared by centrifugation (100 *g*, 15 min, 22 °C), and the resulting PRP was mixed with a 15% volume of ACD solution. The PRP was centrifuged (2200 *g*, 7 min, 22 °C), and the platelet pellet was obtained by removing the supernatant. The pellet was resuspended in platelet-poor plasma (PPP) prepared by centrifugation (2200 *g*, 10 min, 22 °C), and the platelet count was adjusted from $1{\cdot}0 \times 10^5$ per microlitre to $1{\cdot}0 \times 10^6$ per microlitre using an automated haematology analyser (K-4500). The anaesthetized rabbits with severe thrombocytopenia were cannulated on day 15 with a 23-gauge scalp vein infusion set, and the various PRPs with defined platelet counts were transfused into the ear vein by an infusion pump at a rate of 0·5 mL $min^{-1}$ and at a dose of 4 mL $kg^{-1}$. Platelet recovery at 30 min was calculated as described previously (Michelson *et al.*, 1996), using an estimated blood volume of 58 mL $kg^{-1}$ (Reimers *et al.*, 1973).

We also confirmed that the transfused platelets had a normal half-life period and survival time (The Panel on Diagnostic Application of Radioisotopes in Hematology, International Committee for Standardization in Hematology, 1977) in the blood circulation as follows: the PRP was mixed with 15% (v/v) of ACD and centrifuged (2200 *g*, 10 min, 22 °C). The plasma supernatants were replaced with a Ringer's citrate–dextrose solution [RCD solution, composition: 0·76% (w/v) citric acid, 0·090% (w/v) glucose, 0·043% (w/v) $MgCl_2$, 0·038% (w/v) KCl and 0·60% (w/v) NaCl, pH 6·5]. After resuspension, this mixture was added drop by drop to a 10 mM solution of NHS–biotin in DMSO (to a final concentration of 10 μM) and was incubated at 37 °C for 30 min. The suspension washed with the RCD solution by centrifugation (2200 *g*, 7 min, 22 °C), and the biotin-labelled PRP was resuspended to $5{\cdot}0 \times 10^5$ per microlitre in PPP prepared by centrifugation (2200 *g*, 10 min, 22 °C). Using a similar method as before, the resulting PRP was transfused into the ear vein using a 23-gauge scalp vein infusion set, and 200 μL blood was collected from the ear vein at time intervals using a 23-gauge needle. This was then mixed with ACD [final concentration 10% (v/v)], followed by centrifugation (100 *g*, 10 min, 22 °C). Ten microlitres PE–streptavidin (1 : 20 dilution of 0·5 mg $mL^{-1}$ solution in PBS) was added to 50 μL platelet suspension, followed by incubation for 30 min at room temperature before fixing with paraformaldehyde [final concentration 1·0% (w/v)]. The platelets were gated to their characteristic forward vs. side scatter, and $1{\cdot}0 \times 10^4$ platelets were analysed using a FACS-Calibur flow cytometer (Nihon Becton Dickinson, Tokyo, Japan). The transfused platelets were quantified as a fraction of the PE-positive platelets, and the number of labelled platelets was calculated as the percentage of the circulating labelled platelets. Each experiment was performed at least three times. The platelet survival time was calculated using the 30-min recovery as 100%, as recommended by the Panel on Diagnostic Application of Radioisotopes in Hematology, International Committee for Standardization in Hematology (1977).

*Measurement of the ear bleeding time*

The anaesthetized thrombocytopenic rabbits were cannulated on day 15 with a 23-gauge scalp vein infusion set, and the sample suspension (10, 20 and 30 mg $mL^{-1}$ equivalent of rHSA) was infused into the ear vein using an infusion pump at a rate of 0·5 mL $min^{-1}$. The samples were the H12–PEG–polyAlb and the PEG–polyAlb at a dose of 4 mL $kg^{-1}$, and saline was used to obtain the control value. Thirty minutes

after administration, a 6-mm-length standardized incision (No. 11 scalpel blade; AS ONE Co., Osaka, Japan) was made at a site where no vessel was visible. The ear was immersed in a saline bath, and the time until the bleeding stopped was measured. In the case of bleeding over 30 min, we registered the bleeding time as 30 min. In addition, cell counts were determined using an automated haematology analyser (K-4500) before (−5 min) and after (60 min) injection of samples.

*Measurement of blood coagulation parameters*

Blood withdrawn from thrombocytopenic rabbits after injection of the H12–PEG–polyAlb, the PEG–polyAlb or saline was mixed with a 10% volume of 3·8% (w/v) sodium citrate, and the plasma was collected by centrifugation (2200 *g*, 10 min, room temperature). The clinical laboratory testing such as prothrombin time (PT), activated partial thromboplastin time (APTT) and fibrinogen antigen (Fbg) was carried out by SRL, Inc. (Tokyo, Japan).

*Statistical analyses*

A statistical evaluation of various counts of the PRP group vs. the PPP group is shown in Fig. 2. A comparison of the H12–PEG–polyAlb group vs. the PEG-polyAlb or the saline group as shown in Fig. 3 was also carried out using Tukey–Kramer tests. A $P$ value of less than 0·05 was considered to be statistically significant. Statistical analyses were performed using StatView software (HULINKS Inc., Tokyo, Japan).

## RESULTS

*Characterization of H12–PEG–polyAlb*

We modified the surface of polyAlb particles (diameter of 240 ± 100 nm) with MALPEG and mPEG, and the number of MALPEG and mPEG molecules that chemically bound to one polyAlb particle was estimated to be approximately $1{\cdot}2 \times 10^4$ and $6{\cdot}1 \times 10^4$ molecules, respectively, by the indirect quantification of free PEG molecules. Furthermore, the number of H12 conjugated per polyAlb was estimated to be approximately $1{\cdot}0 \times 10^4$. The endotoxin concentration in the suspension of H12–PEG–polyAlb at an rHSA concentration of 10 mg $mL^{-1}$ was below 0·25 EU $mL^{-1}$, and this was acceptable for the *in vivo* study.

*Busulphan-induced thrombocytopenic rabbits*

Rabbits that received busulphan at total doses of 40 and 50 mg $kg^{-1}$ developed profound thrombocytopenia with a decline in platelet count to the half-maximal value on day 7, and the count reached the lowest value on days 15 and 14, respectively (Fig. 1). However, the haematocrit and leucocytes of these rabbits also decreased, and the rabbits became anaemic and purpuric as shown in Table 1. On the other hand, at a total dose of 30 mg $kg^{-1}$, thrombocytopenia was just as profound as at the higher doses of busulphan, and the rabbits showed a decline in platelet count to the half-maximal value on day 7. On days 13, 14 and 15, the platelet counts were $6{\cdot}9 \pm 0{\cdot}1$, $3{\cdot}5 \pm 1{\cdot}0$ and $2{\cdot}4 \pm 1{\cdot}3 \times 10^4$ per microlitre, respectively, which were equivalent to 1/15 or 1/20 of the platelet counts of normal rabbits ($37{\cdot}3 \pm 7{\cdot}6 \times 10^4$ per microlitre). There was a slight decrease in the leucocyte counts of the busulphan-treated rabbits compared with normal rabbits, and the haematocrits were unchanged, as shown in Table 1. After the platelet counts reached their lowest point on day 15, the count persisted for at least 1 day, then gradually started to rise, and recovered to the normal level on day 20. Consequently, for the *in vivo* experiment, we used rabbits having the most severe thrombocytopenia on day 15 after the busulphan treatment to evaluate the haemostatic ability of H12–PEG–polyAlb.

*Platelet transfusion and measurement of ear bleeding time*

When the PRP with counts of $0{\cdot}4 \times 10^9$, $1{\cdot}2 \times 10^9$, $2{\cdot}0 \times 10^9$ and $4{\cdot}0 \times 10^9$ per kilogram ($1{\cdot}0 \times 10^5$,

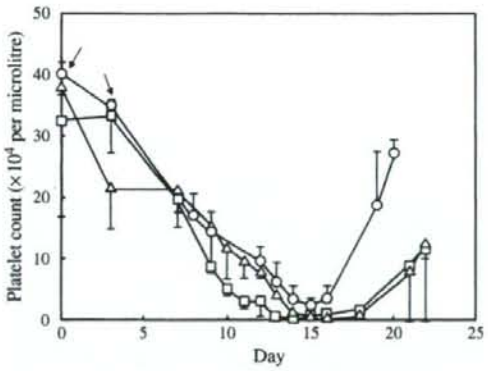


**Fig. 1.** Dose–response effect of busulphan on rabbits. Rabbits were treated with busulphan at a total dose of 30 mg $kg^{-1}$ (○), 40 mg $kg^{-1}$ (△) or 50 mg $kg^{-1}$ (□). Ear vein blood was collected at defined intervals and platelet counts were measured. Arrows indicate the injection day of busulphan ($n$ = 3).

 

**Table 1.** Haematological parameters on day 15 after busulphan injection

| | Haematocrit (%) | White blood cell ($\times 10^3$ per microlitre) | Platelet ($\times 10^4$ per microlitre) |
|---|---|---|---|
| Normal | 33·5 ± 4·2 | 3·1 ± 1·2 | 37·3 ± 7·6 |
| Busulphan 30 mg kg$^{-1}$ | 31·3 ± 2·1 | 3·0 ± 1·8 | 2·4 ± 1·3 |
| Busulphan 40 mg kg$^{-1}$ | 27·7 ± 4·0 | 2·7 ± 1·0 | 0·4 ± 0·1 |
| Busulphan 50 mg kg$^{-1}$ | 26·6 ± 3·1 | 1·7 ± 1·5 | 1·0 ± 0·3 |

$3.0 \times 10^5$, $5.0 \times 10^5$, and $1.0 \times 10^6$ per microlitre at a dose of 4 mL kg$^{-1}$, respectively) was transfused intravenously into the thrombocytopenic rabbits (platelet = $2.1 \pm 0.5 \times 10^4$ per microlitre), the platelet counts gradually increased with time, reaching maximal values 30 min after transfusion, which were $2.2 \pm 1.1$, $3.2 \pm 0.9$, $4.0 \pm 1.1$ and $6.1 \pm 0.8 \times 10^4$ per microlitre, respectively (Fig. 2). The mean percentages of recovery at 30 min after transfusion were calculated to be 65·1 ± 14·8, 65·4 ± 22·1, 66·7 ± 15·8 and 76·6 ± 9·2%, respectively. Furthermore, the half-life and survival time of transfused platelets at a dose of $2.0 \times 10^9$ per kilogram were estimated to be 39·1 ± 6·1 and 56·4 ± 5·5 h, respectively. However, the platelet count did not change before and after PPP transfusion.

The ear bleeding times of the normal rabbits (platelet = $37.3 \pm 7.6 \times 10^4$ per microlitre) and the thrombocytopenic rabbits (platelet = $2.4 \pm 1.3 \times 10^4$ per microlitre) after the saline injection were 112 ± 24 and 1695 ± 197 s, respectively (Fig. 3). The bleeding time of the thrombocytopenic rabbits was approximately 15 times longer than that of the normal rabbits. The bleeding time at 30 min after PPP transfusion was 1473 ± 442 s, which was almost comparable to that obtained with the control thrombocytopenic rabbits injected with saline. At doses of $0.4 \times 10^9$, $1.2 \times 10^9$, $2.0 \times 10^9$ and $4.0 \times 10^9$ per kilogram, there was a dose-dependent reduction in the bleeding time of the PRP, and the bleeding time was significantly reduced to 1505 ± 410, 863 ± 540, 867 ± 440 and 505 ± 257 s, respectively (Fig. 2).

*Haemostatic effects of the H12–PEG–polyAlb*

When the H12–PEG–polyAlb at the dose of 40 mg kg$^{-1}$ was injected into the thrombocytopenic rabbits, the bleeding time was not reduced (1416 ± 533 s) and was comparable to the that of control PEG-polyAlb at a dose of 40 mg kg$^{-1}$ (1431 ± 402 s), as shown in Fig. 3. However, intravenous administration of the H12–PEG–polyAlb at a dose of 80 mg kg$^{-1}$ significantly reduced the bleeding time to 834 ± 266 s compared with administration of saline (1695 ± 197 s) or the control PEG–polyAlb (1592 ± 286 s) at a dose of 80 mg kg$^{-1}$. At a dose of 120 mg kg$^{-1}$, the H12–PEG–polyAlb also significantly reduced the bleeding time to

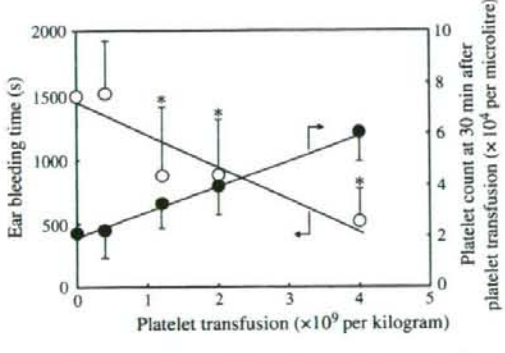


**Fig. 2.** Effects of platelet transfusion on ear bleeding time (○). The transfused amounts of platelets were $0.4 \times 10^9$, $1.2 \times 10^9$, $2.0 \times 10^9$ and $4.0 \times 10^9$ per kilogram. Platelet count in the rabbits at 30 min after platelet transfusion (●) ($n = 6$).
*$P < 0.05$ vs. PPP group.

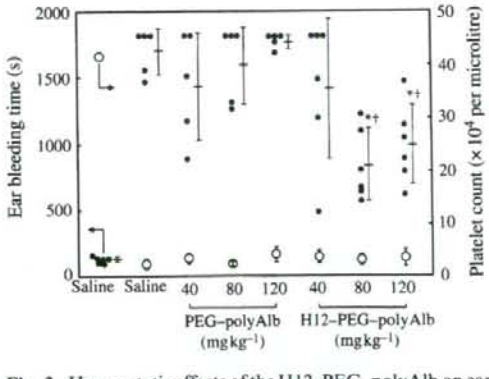


**Fig. 3.** Haemostatic effects of the H12–PEG–polyAlb on ear bleeding time (●). The administered amount of H12–PEG–polyAlb was 40, 80 and 120 mg kg$^{-1}$ equivalent of rHSA. (○)indicates platelet count in the rabbits ($n = 5$–6).
*$P < 0.05$ vs. saline group, and †$P < 0.05$ vs. PEG–polyAlb group at the same dose.

 

990 ± 294 s compared with the control PEG–polyAlb (1772 ± 49 s), and the reduction effect was comparable to the response to the H12–PEG–polyAlb at a dose of 80 mg $kg^{-1}$.

*Measurement of blood coagulation parameters*

Three blood coagulation parameters, PT, APTT and Fbg, were evaluated for the rabbit blood approximately 60 min after the measurement of bleeding time, as listed in Table 2. No significant difference was seen between the sample groups (H12–PEG–polyAlb and PEG–polyAlb) and the control saline group, indicating no influence of the H12–PEG–polyAlb particles on the endogenous and exogenous coagulation activities.

## DISCUSSION

We previously succeeded in prolonging the *in vivo* blood residence time of H12-conjugated polyAlb by PEG modification (H12–PEG–polyAlb), and we confirmed that the H12–PEG–polyAlb maintained an ability to specifically bind activated platelets (Okamura *et al.*, 2007). Furthermore, the H12–PEG–polyAlb dose dependently shortened the tail bleeding time of rats with moderate thrombocytopenia (Okamura *et al.*, 2007). In this study, we have evaluated the haemostatic effects of H12–PEG–polyAlb as a platelet substitute using larger animals with severe thrombocytopenia (thrombocytopenic rabbits).

We conjugated H12 to the surface of polyAlb particles modified with PEG chains, estimating the conjugation density on the polyAlb surface as approximately $4{\cdot}6 \times 10^4$ molecules $\mu m^{-2}$. We previously confirmed that the conjugation density of H12 over $4{\cdot}6 \times 10^4$ molecules $\mu m^{-2}$ needs to maintain binding ability towards activated platelets, based on the flow cytometric analyses (Okamura *et al.*, 2005b, 2007). The density was similar to that of the H12–PEG–polyAlb in our previous studies, which enhanced thrombus formation under the *in vitro* flow conditions and significantly reduced the tail bleeding time of thrombocytopenic rats. However, the number of GPIIb/IIIa on one platelet is approximately $8{\cdot}0 \times 10^4$ molecules, of which density is calculated to be approximately $4{\cdot}1 \times 10^3$ molecules $\mu m^{-2}$ based on the diameter of typical platelet (approximately 2·5 μm), referring to a report by Wagner *et al.* (1996). Consequently, the conjugation number of H12 on the surface of the polyAlb particle was 10-fold level in comparison with that of GPIIb/IIIa.

Next, we induced severe thrombocytopenia in the rabbits using busulphan in order to evaluate the haemostatic ability of the H12–PEG–polyAlb *in vivo*. We obtained a platelet extinction curve similar to that seen in previous studies (Kuter & Rosenberg, 1995). Sola *et al.* (2001) previously reported that a low haematocrit resulted in a significant prolongation in the bleeding time. In fact, the bleeding times on day 15 of all rabbits that received busulphan at total doses of 40 or 50 mg $kg^{-1}$ were not measurable because the bleeding did not stop for more than 30 min (data not shown). From the haematological indices data in shown in Table 1, we evaluated conditions producing a low platelet count but maintaining a constant haematocrit value, and we determined that the appropriate busulphan dose was 30 mg $kg^{-1}$ for the rabbits. Furthermore, the bleeding time of the thrombocytopenic rabbits on day 15 was significantly extended in comparison with that of the normal rabbits and the thrombocytopenic rabbits on day 13 or 14 (data not shown). We decided that the ear incision was to be made on day 15 and prepared the severely thrombocytopenic rabbits.

We judged that there are specific haemostatic effects when H12–PEG–polyAlb was significantly reduced the ear bleeding time of thrombocytopenic rabbits in comparison with saline and control PEG–polyAlb (H12 non-conjugation) groups. Using these rabbits, we confirmed the significant haemostatic effect of the H12–PEG–polyAlb at the doses of 80 and 120 mg $kg^{-1}$, although a dose-dependent reduction was not observed, as shown in Fig. 3. However, the H12–PEG–polyAlb at a dose of 40 mg $kg^{-1}$ did not produce this effect. We previously reported a significant haemostatic effect of H12–PEG–polyAlb at a dose of 40 mg $kg^{-1}$ using rats with moderate thrombocytopenia (Okamura *et al.*, 2007). The present results indicate that a higher dose of the H12–PEG–polyAlb was necessary to assist platelet haemostasis in the

**Table 2.** Blood coagulation parameters after administration of H12–PEG–polyAlb at a dose of 80 mg $kg^{-1}$

| | PT (s) | APTT (s) | Fbg (g $dL^{-1}$) |
|---|---|---|---|
| Saline (normal) | 8·1 ± 0·2 | 26·1 ± 1·2 | 256·6 ± 15·3 |
| Saline (thrombocytopenia) | 8·3 ± 0·6 | 23·6 ± 5·3 | 259·7 ± 15·2 |
| PEG–polyAlb | 8·5 ± 0·5 | 26·1 ± 2·0 | 264·2 ± 26·6 |
| H12–PEG–polyAlb | 8·4 ± 0·4 | 24·7 ± 3·8 | 267·8 ± 10·3 |

 

severe thrombocytopenia model. Based on our previous studies of the H12 particles under flow conditions *in vitro* (Takeoka *et al.*, 2003), we hypothesized that the H12–PEG–polyAlb would work at the vascular injury by the following mechanisms: (1) adhesion of the H12–PEG–polyAlb could be initiated by the activated platelets, which had already adhered on the surface of the exposed collagen at the vascular injury, (2) the H12–PEG–polyAlb adhering to the surface of the platelet could provide additional binding sites for activated platelets and (3) the H12–PEG–polyAlb could accelerate thrombus formation by enhancing aggregation of the flowing platelets. However, in the case of severe thrombocytopenia, adhesion of the H12–PEG–polyAlb decreased because the fewer platelets adhered on the collagen. It was suggested that higher doses of the H12–PEG–polyAlb would be necessary to assist platelet haemostasis by recruiting the flowing platelets and filling up the vascular injury site using the volume of the H12–PEG–polyAlb particles. However, considering the dose-independent reduction of the particles, it was also suggested that there was a limited time window for the H12–PEG–polyAlb to accumulate and fill up the vascular injury site and that additional processes such as amplification of platelet aggregation and blood coagulation would be necessary to further promote platelet haemostasis.

Furthermore, we also confirmed that haematological indices (data not shown) and coagulation parameters as shown in Table 2 did not change before and after the infusion of the H12–PEG–polyAlb, suggesting that the polyAlb was a safe particle with a minimal likelihood of causing side effects after injection.

We used a platelet transfusion model as a positive control for the platelet substitutes. The survival time of the transfused platelets was comparable to that obtained from the $^{51}$Cr and $^{111}$In-labelled platelets evaluated in previous reports (Packham *et al.*, 1992; Franco *et al.*, 1994), whereas the mean percentage of recovery was similar to the that in previous reports (Packham *et al.*, 1992; Franco *et al.*, 1994; Rand *et al.*, 2002). Furthermore, confirmation of a dose-dependent reduction in the bleeding time after administering PRP to severe thrombocytopenic rabbits established a positive control for comparison with platelet substitutes. We proposed the following equation (Eqn 1) relating the transfused platelet counts to the bleeding time as follows:

$$y = -252{\cdot}03x + 1425{\cdot}6 (r^2 = 0{\cdot}85) \qquad (1)$$

where the $x$ value gives the PRP ($10^9$ per kilogram) and $y$ value gives the ear bleeding time (s). We estimated the haemostatic capacity of H12–PEG–polyAlb using Eqn 1. The bleeding time (834 ± 266 s) of the H12–PEG–polyAlb at a dose of 80 mg kg$^{-1}$ (approximately $7{\cdot}4 \times 10^{13}$ particles kg$^{-1}$) was similar to that following platelet transfusion at a dose of $2{\cdot}4 \times 10^9$ per kilogram. Similarly, in the case of 120 mg kg$^{-1}$ (approximately $1{\cdot}1 \times 10^{14}$ particles kg$^{-1}$), the bleeding time of the H12–PEG–polyAlb was similar to that of platelet transfusion at a dose of $1{\cdot}7 \times 10^9$ per kilogram. These results indicate the haemostatic capacity of the H12–PEG–polyAlb at the particle number $3{\cdot}1 \times 10^4$ to $6{\cdot}5 \times 10^4$ would correspond to that of one platelet. We also evaluated the haemostatic capacity based on the total injected particle volume because the particle diameter of the H12–PEG–polyAlb (240 ± 100 nm) is 10-fold smaller than that of a typical platelet (2–3 μm). We calculated that the volume of the particles required for haemostatic support was 31- to 65-fold less than that of platelets that would produce a similar effect.

In conclusion, the H12–PEG–polyAlb significantly shortened the ear bleeding time of severely thrombocytopenic rabbits. We assessed the haemostatic capacity of the H12–PEG–polyAlb based on comparisons with platelet transfusions and calculated that the haemostatic capacity of the H12–PEG–polyAlb was approximately 31- or 65-fold greater than that of a similar volume of platelets. Thus, the H12–PEG–polyAlb may be a suitable candidate for an alternative to human platelet concentrates infused to treat bleeding in patients with severe thrombocytopenia. In future, we plan to assess the haemostatic ability of the H12–PEG–polyAlb to treat animals with severe thrombocytopenia resulting from blood loss during surgery.

## ACKNOWLEDGMENTS

The authors thank M. Murata, MD, PhD, and K. Yokoyama, MD, PhD, at Keio University for useful discussion about the functional evaluation of H12 peptide and blood coagulation parameters. This work was supported in part by Health and Labor Sciences Research Grants (Research on Pharmaceutical and Medical Safety, S. T., Y. I. and M. H.), Ministry of Health, Labor and Welfare, Japan. Y. O. was the recipient of Japan Health Sciences Foundation. T. F. was the scholar 'Doctor-21' of Yoshida Scholarship Foundation.

## REFERENCES

Agam, G. & Livine, A.A. (1992) Erythrocytes with covalently bound fibrinogen as a cellular replacement for

 

the treatment of thrombocytopenia. *European Journal of Clinical Investigation*, **22,** 105–112.

Casals, E., Verdaguer, A., Tonda, R., Galan, A., Escolar, G. & Estelrich, J. (2003) Atomic force microscopy of liposomes bearing fibrinogen. *Bioconjugate Chemistry*, **14,** 593–600.

Coller, B.S., Springer, K.T., Beer, J.H., Mohandas, N., Scudder, L.E., Norton, K.J. & West, S.M. (1992) Thromboerythrocytes. In vitro studies of a potential autologous, semi-artificial alternative to platelet transfusion. *Journal of Clinical Investigation*, **89,** 546–555.

De Marco, L., Girolami, A. & Zimmerman, T.S. (1986) Von Willebrand factor interaction with the glycoprotein IIb/IIIa complex. *Journal of Clinical Investigation*, **77,** 1272–1277.

Franco, R.S., Lee, K.N., Barker-Gear, R., Gates, R. & Menitove, J.E. (1994) Use of bi-label biotinylation for concurrent measurement of in vivo recovery and survival in two rabbit platelet populations. *Transfusion*, **34,** 784–789.

Graham, S.S., Gonchoroff, N.J. & Miller, J.L. (2001) Infusible platelet membranes retain partial functionality of the platelet GPIb/IX/V receptor complex. *American Journal of Clinical Pathology*, **115,** 144–147.

Kitaguchi, T., Murata, M., Iijima, K., Kamide, K., Imagawa, T. & Ikeda, Y. (1999) Characterization of liposomes carrying von Willebrand factor-binding domain of platelet glycoprotein Ibα: a potential substitute for platelet transfusion. *Biochemical and Biophysical Research Communications*, **261,** 784–789.

Kloczewiak, M., Timmons, S. & Hawiger, J. (1982) Localization of a site interacting with human platelet receptor on carboxy-terminal segment of human fibrinogen γ chain. *Biochemical and Biophysical Research Communications*, **107,** 181–187.

Kloczewiak, M., Timmons, S., Lukas, T.J. & Hawiger, J. (1984) Platelet receptor recognition site on human fibrinogen. Synthesis and structure-function relationship of peptides corresponding to the carboxy-terminal segment of the γ chain. *Biochemistry*, **23,** 1767–1774.

Kloczewiak, M., Timmons, S., Bednarek, M.A., Sakon, M. & Hawiger, J. (1989) Platelet receptor recognition domain on the γ chain of human fibrinogen and its synthetic peptide analogues. *Biochemistry*, **28,** 2915–2919.

Kuter, D.J. & Rosenberg, R.D. (1995) The reciprocal relationship of thrombopoietin (c-Mpl ligand) to changes in the platelet mass during busulfan-induced thrombocytopenia in the rabbit. *Blood*, **85,** 2720–2730.

Lam, S.C., Plow, E.F., Smith, M.A., Andrieux, A., Ryckwaert, J.J., Marguerie, G. & Ginsberg, M.H. (1987) Evidence that arginyl-glycyl-aspartate peptides and γ chain peptides share a common binding site on platelets. *Journal of Biological Chemistry*, **262,** 110–115.

Levi, M., Friedrich, P.W., Middleton, S. *et al.* (1999) Fibrinogen-coated albumin microcapsules reduce bleeding in severely thrombocytopenic rabbits. *Nature Medicine*, **5,** 107–111.

Michelson, A.D., Barnard, M.R., Hechtman, H.B., MacGregor, H., Connolly, R.J., Loscalzo, J. & Valeri, C.R. (1996) In vivo tracking of platelets: circulating degranulated platelets rapidly lose surface P-selectin but continue to circulate and function. *Proceedings of National Academy of Sciences of the United State of America*, **93,** 11877–11882.

Mustard, J.F., Packham, M.A. & Kinlough-Rathbone, R.L. (1978) Fibrinogen and ADP-induced platelet aggregation. *Blood*, **52,** 453–466.

Nishiya, T., Kainoh, M., Murata, M., Handa, M. & Ikeda, Y. (2002) Reconstitution of adhesive properties of human platelets in liposomes carrying both recombinant glycoproteins Ia/IIa and Ibα under flow conditions: specific synergy of receptor-ligand interactions. *Blood*, **100,** 136–142.

Okamura, Y., Maekawa, Y., Teramura, Y., Maruyama, H., Handa, H., Ikeda, Y. & Takeoka, S. (2005a) Hemostatic effects of phospholipid vesicles carrying fibrinogen-γ chain dodecapeptide in vitro and in vivo. *Bioconjugate Chemistry*, **16,** 1589–1596.

Okamura, Y., Takeoka, S., Teramura, Y., Maruyama, H., Tsuchida, E., Handa, M. & Ikeda, Y. (2005b) Hemostatic effects of fibrinogen γ-chain dodecapeptide-conjugated polymerized albumin particles in vitro and in vivo. *Transfusion*, **45,** 1221–1228.

Okamura, Y., Fujie, T., Maruyama, H., Handa, M., Ikeda, Y. & Takeoka, S. (2007) Prolonged hemostatic ability of poly(ethylene glycol)-modified polymerized albumin particles carrying fibrinogen γ-chain dodecapeptide. *Transfusion*, **47,** 1254–1262.

Packham, M.A., Rand, M.L. & Kinlough-Rathbone, R.L. (1992) Similarities and differences between rabbit and human platelet characteristics and functions. *Comparative Biochemistry and Physiology A*, **103,** 35–54.

Rand, M.L., Wang, H., Mody, M., Chu, I., Treutiger, I., Nguyen, A., Packham, M.A. & Freedman, J. (2002) Concurrent measurement of the survival of two populations of rabbit platelets labeled with either two PKH lipophilic dyes or two concentrations of biotin. *Cytometry*, **47,** 111–117.

Reimers, H.J., Buchanan, M.R. & Mustard, J.F. (1973) Survival of washed rabbit platelets in vivo. *Proceedings of the Society for Experimental Biology and Medicine*, **142,** 1222–1225.

Ruggeri, Z.M., De Marco, L. & Gatti, L. (1983) Platelets have more than one binding site for von Willebrand factor. *Journal of Clinical Investigation*, **72,** 1–12.

Rybak, M. & Renzulli, L.A. (1993) A liposome based platelet substitutes, the plateletsome, with hemostatic efficacy. *Biomaterials, Artificial Cells, and Immobilization Biotechnology*, **21,** 108–118.

Sola, M.C., del Vecchio, A., Edwards, T.J., Suttner, D., Huston, A.D. & Christensen, R.D. (2001) The relationship between hematocrit and bleeding time in very low birth weight infants during the first week of life. *Journal of Perinatology*, **21,** 368–371.

 

Takagi, J., Petre, B.M., Walz, T. & Springer, T.A. (2002) Global conformational rearrangements in integrin extracellular domains in outside-in and inside-out signaling. *Cell*, **110,** 599–611.

Takeoka, S., Teramura, Y., Ohkawa, H., Ikeda, Y. & Tsuchida, E. (2000) Conjugation of von Willebrand factor-binding domain of platelet glycoprotein Ibα to size-controlled albumin microspheres. *Biomacromolecules*, **1,** 290–295.

Takeoka, S., Teramura, Y., Okamura, Y., Handa, M., Ikeda, Y. & Tsuchida, E. (2001) Fibrinogen-conjugated albumin polymers and their interaction with platelets under flow conditions. *Biomacromolecules*, **2,** 1192–1197.

Takeoka, S., Teramura, Y., Okamura, Y., Tsuchida, E., Handa, M. & Ikeda, Y. (2002) Rolling properties of rGPIbα-conjugated phospholipid vesicles with different membrane flexibilities on vWf surface under flow conditions. *Biochemical and Biophysical Research Communications*, **296,** 765–770.

Takeoka, S., Okamura, Y., Teramura, Y., Watanabe, N., Suziki, H., Tsuchida, E., Handa, M. & Ikeda, Y. (2003) Function of fibrinogen γ-chain dodecapeptide-conjugated latex beads under flow. *Biochemical and Biophysical Research Communications*, **312,** 773–779.

Teramura, Y., Okamura, Y., Takeoka, S. *et al.* (2003) Hemostatic effects of polymerized albumin particles bearing rGPIa/IIa in thrombocytopenic mice. *Biochemical and Biophysical Research Communications*, **306,** 256–260.

The Panel on Diagnostic Application of Radioisotopes in Hematology, International Committee for Standardization in Hematology. Recommended methods for radioisotope platelet survival studies. (1977) *Blood*, **50,** 1137–1144.

Wagner, C.L., Mascelli, M.A., Neblock, D.S., Weisman, H.F., Coller, B.S. & Jordan, R.E. (1996) Analysis of GPIIb/IIIa receptor number by quantification of 7E3 binding to human platelets. *Blood*, **88,** 907–914.

Wertheimer, E., Shapiro, B. & Fodor-Salomonowicz, I. (1944) Stability of fibrinogen in normal and pathological plasma. *British Journal of Experimental Pathology*, **25,** 121–125.

Xiao, T., Takagi, J., Coller, B.S., Wang, J.H. & Springer, T.A. (2004) Structural basis for allostery in integrins and binding to fibrinogen-mimetic therapeutics. *Nature*, **432,** 59–67.

 

# Fabrication of free-standing albumin-nanosheets having heterosurfaces

**Yosuke Okamura, Takahiro Goto, Daisuke Niwa, Yoshihito Fukui, Masanobu Otsuka, Norikazu Motohashi, Tetsuya Osaka, Shinji Takeoka**

*Consolidated Research Institute for Advanced Science and Medical Care, Waseda University, Tokyo 169-8555, Japan*

Received 2 August 2007; revised 11 December 2007; accepted 11 December 2007
Published online 22 April 2008 in Wiley InterScience (www.interscience.wiley.com). DOI: 10.1002/jbm.a.31934

**Abstract:** Sheet-shaped carriers, having both obverse and reverse surfaces and thus a large contact area for targeting a site, have several advantages over spherical-shaped carriers, which have an extremely small contact area for targeting sites. Here, we proposed a novel method to prepare a free-standing ultrathin and biocompatible nanosheet having heterosurfaces, by a combination of four processes: (1) specific adsorption of recombinant human serum albumin (rHSA) molecules onto a patterned octadecyltrimethoxysilane self-assembled monolayer region (ODS-SAM), (2) preparation of nanosheets of rHSA molecules bearing thiol groups (SH-rHSA) via two-dimensionally disulfide crosslinking, (3) surface modification of the resulting nanosheet, and (4) preparation of the free-standing nanosheet by detachment from the ODS-SAM. The SH-rHSA molecules at pH 5.0 and a concentration of 1 μg/mL were specifically adsorbed on the patterned ODS-SAM regions by hydrophobic interaction, and were two-dimensionally crosslinked in the presence of copper ion as an oxidant. The rHSA-nanosheets were then simply detached from the ODS-SAM by treatment with surfactant. We succeeded in the preparation of rectangular (10 μm × 30 μm) and ultrathin (4.5 ± 1.0 nm) rHSA-nanosheets on a patterned ODS-SAM, and could also obtain free-standing rHSA-nanosheets having heterosurfaces by surface modification with fluorescent latex beads. Thus, the rHSA-nanosheets having heterosurfaces could be regarded as a new biomaterial for drug carriers, hemostatic reagents, wound dressing for burn injury, and so forth. © 2008 Wiley Periodicals, Inc. J Biomed Mater Res 89A: 233–241, 2009

**Key words:** albumin; nanosheet; free-standing; biocompatibility; crosslinking

## INTRODUCTION

In recent years, much attention has been paid to drug-delivery system (DDS) as a new pharmacological approach to improve the efficacy and safety of drugs. In DDS, vesicles, micelles, emulsions, and biodegradable nanoparticles have been extensively studied as carriers for biologically active substances such as drugs, recognition proteins, enzymes, genes, and so forth.[1] There are two concepts for the development of DDS: passive and active targeting systems. In the latter case, recognition proteins such as antibodies and various ligands are conjugated to the surface of the carriers to target the tissue epitopes or specific cells.

We have developed biocompatible and biodegradable nanoparticles such as albumin-based nanoparticles[2–5] and phospholipid vesicles[6,7] carrying recombinant fragments of platelet membrane proteins[3,4,6,8] and dodecapeptide as a recognition site for fibrinogen.[2,5,7,9] These nanoparticles specifically recognized the site of bleeding injury or activated platelets. In our approach to the conjugation of high- and low-molecular-weight molecules such as glycoprotein Ibα and dodecapeptide to the surface of the particle, we observed that the activity of dodecapeptide was suppressed by the steric hindrance of the glycoprotein Ibα, and found that a spacer such as a poly(ethylene glycol) chain was needed in the conjugation of the peptides.[8]

On the other hand, sheet-shaped carriers, having both obverse and reverse surfaces and thus a large contact area for targeting a site, have several advantages over spherical-shaped carriers, which have an extremely small contact area for targeting sites. Recently, several approaches have been implemented for the fabrication of free-standing films, combining large surface area with nanoscale thickness, from polymers and/or from inorganic materials: cast films,[10] layer-by-layer assemblies of polyelectolyte multilayers,[11–15] crosslinked amphiphilic Langmuir–Blodgett films,[16] self-assembled monolayers (SAMs),[17,18] and assemblies of triblock copolymers.[19] However, there

*Correspondence to:* S. Takeoka; e-mail: takeoka@waseda.jp
Contract grant sponsor: Shorai Foundation for Science and Technology

have been no reports on the preparation of free-standing nanoscale sheets from biocompatible and biodegradable materials only. The nanosheets would be a candidate as a new injectable biomaterial in DDSs.

Organosilane SAMs have been widely applied to control physical and chemical properties of the surfaces of glass, quartz, $SiO_2$/Si wafers, or silica particles.[20] Furthermore, they are excellent tools to study the immobilization of proteins such as redox proteins,[21] enzymes,[22] and immunoglobulins, using covalent bonds or noncovalent bonds such as ionic or hydrogen bonds, van der Waals attraction, and hydrophobic interaction with the various terminal groups of SAMs. Generally, it is easy to construct patterned SAMs with uniform sizes and shapes on silicon oxide or gold substrates using conventional photolithography processes.[23] This approach was used for the electrochemical analysis of proteins immobilized by adsorption on the substrates.

Here, we proposed a novel method to prepare a free-standing biocompatible nanosheet having heterosurfaces. We used a patterned hydrophobic octadecyltrimethoxysilane-SAM (ODS-SAM) on silicon oxide to prepare nanosheets of uniform sizes and shapes. Furthermore, we modified the surface of the nanosheet with fluorescent latex beads as a model material to prove the fabrication of a nanosheet with heterosurfaces.

## MATERIALS AND METHODS

### Reagents

P-type Si (100) wafers (below 0.02 Ω cm) covered with thermally grown silicon oxide (~200 nm) was purchased from KST World, Co. (Fukui, Japan). *n*-Octadecyltrimethoxysilane (ODS, 97%) was purchased from Gelest (Morrisville, PA). Succinimidyl 6-[3′-(2-pyridyldithio) propionamido] hexanoate (LC-SPDP) and *N*-(ε-maleimidocaproyl) succinimide ester (EMCS) were purchased from Pierce Biotechnology (Rockford, IL). Dithiothreitol (DTT) and copper sulfate pentahydrate were purchased from Wako Pure Chemical Industries (Osaka, Japan). 5,(6)-Tetramethylrhodamine isothiocyanate (TRITC) and 7-chloro-4-nitrobenzo-2-oxa-1,3-diazole (NBD) were purchased from Invitrogen (Carlsbad, CA). Sephadex G25 for gel permeation chromatography (GPC) was purchased from GE Healthcare UK (Buckinghamshire, England). Latex beads (Polybead™, 100 nm ϕ) were purchased from Polysciences (Warrington, PA). Recombinant human serum albumin (rHSA, 250 mg/mL) was kindly donated by Oxgenix Co. (Tokyo, Japan).

### SAM preparation

Silicon wafers were treated with SPM (96% $H_2SO_4$: 30% $H_2O_2$ = 4:1 (v/v)) at 120°C followed by rinsing with distilled water. The resulting wafers were placed in a 20-mL Teflon vial containing a glass cup filled with 200 μL of ODS liquid. The vials were sealed with a cap and then heated for 8 h at a constant temperature of 110°C in a dry room to prepare a hydrophobic ODS-SAM on the silicon oxide.[24]

### Patterning processes

The patterned ODS-SAM having hydrophobic octadecyl regions and hydrophilic silicon oxide regions on the substrate was prepared by a conventional photolithography process. The ODS-SAM on the silicon oxide was covered with a photoresist (OFPR-800 500 cP, Tokyo Ohka Kogyo, Co., Kanagawa, Japan), and was irradiated with a 350-nm UV lamp (MA-10, Mikasa, Tokyo, Japan) using a photomask (size: 1 cm × 1 cm, patterning; rectangle (10 μm × 30 μm), Topic Co., Saitama, Japan). After developing (NMD-3), the substrate was exposed to oxygen plasma (Plasma Reactor PR301, Yamato Scientific Co., Tokyo, Japan) at an input power of 200 W and an oxygen flow rate of 80 sccm for removal of ODS. The photoresist was removed by acetone washing to obtain the patterned ODS-SAM.

### Contact angle measurements

A 3-μL drop of distilled water was placed directly onto the ODS-SAM with a micropipette before and after rHSA adsorption, or after the addition of surfactant as described earlier. The liquid drops were observed with an optical microscope with 5× magnification. All water contact angles represented the mean ± SD of the five measurement values.

### Chemical modification of rHSA with thiol groups

An rHSA solution (250 mg/mL) was diluted to 50 mg/mL with a phosphate buffer solution (pH 7.4). A 50 m*M* solution of LC-SPDP in DMSO (150 μL) was added to the rHSA solution (1 mL), and the solution was incubated for 20 min at r.t. To the rHSA solution, a 10 m*M* TRITC phosphate buffer solution (112.5 μL, pH 7.4) was then added and incubated for 20 min at r.t. The unreacted LC-SPDP (precipitated), TRITC, and the byproducts were separated by centrifugation, and then by GPC with an acetate buffer (pH 5.0) to obtain a pyridyl disulfide-bearing rHSA (PD-rHSA). DTT [final concentration (f.c.) 20 m*M*] was added to the PD-rHSA solution to reduce the PD group to a SH group. The unreacted DTT and the byproducts were separated by GPC with an acetate buffer (pH 5.0), and the fractions of TRITC-labeled thiol-introduced rHSA (TRITC-labeled SH-rHSA) were collected. The number of the SH groups conjugated to one rHSA molecule was determined by the quantification of the 2-thiopyridone (2-TP) at 343 nm that was liberated by the addition of DTT.

### Preparation of rHSA-nanosheets

As shown in Figure 1, the substrate of the patterned ODS-SAM was immersed into an acetate buffer solution

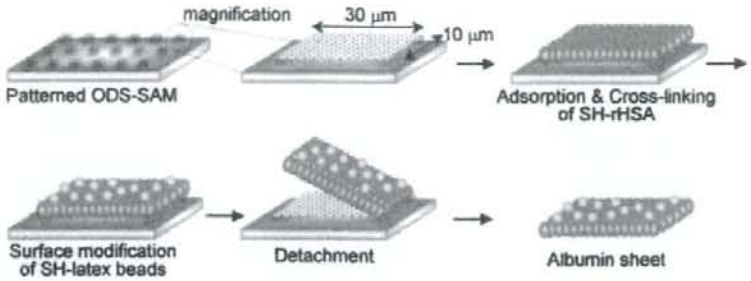


**Figure 1.** Preparation of free-standing rHSA-nanosheets having heterosurfaces on the patterned ODS-SAM. [Color figure can be viewed in the online issue, which is available at www.interscience.wiley.com.]

(pH 5.0) of the TRITC-labeled SH-rHSA at a concentration of 1 μg/mL for 1 h at r.t., and washed with an acetate buffer solution to remove the nonadsorbed SH-rHSA. The substrate was immersed into an acetate buffer solution containing copper ion (II) as a catalyst[25] at a concentration of 1 μ*M* for 12 h at r.t. The series of adsorption, crosslinking, and washing processes were repeated three times. The substrate was immersed into a 1% (v/v) deca(oxyethylene) dodecyl ether ($C_{12}E_{10}$) solution at r.t. for 6 h, to obtain a free-standing rHSA-nanosheet suspension by releasing the rHSA-nanosheets from the substrate. We observed the resulting rHSA-nanosheets using an epifluorescence microscope (ECLIPS TE300, Nikon Co., Tokyo, Japan) equipped with a CCD camera, a confocal laser scanning microscope (LSM 510, Zeiss, Nikon Co.), and an atomic force microscope (AFM) at a tapping mode with a MFP-3D-BIO (Asylum Research, Co., Santa Barbara, CA).

### Conjugation of NBD-labeled latex beads to the surface of rHSA-nanosheets

Latex beads (ϕ 100 nm) were mixed with an rHSA solution (50 mg/mL) and incubated at r.t. for 2 h to coat the surface of the latex bead with rHSA. After the separation of the free rHSA by ultracentrifugation (100,000*g*, 10 min, 4°C, twice), the rHSA-coated latex beads (rHSA-latex beads) were dispersed in a phosphate buffer solution (pH 7.4). The amount of rHSA adsorbed on the surface of the latex bead was analyzed by a microBCA kit (Pierce Biotechnology). A solution of LC-SPDP in DMSO (2 eq. mol with respect to the rHSA adsorbed on the surface of the latex bead) was added to the suspension of the rHSA-latex beads and incubated for 20 min at r.t. The solution of NBD in DMSO (2 eq. mol with respect to rHSA on the surface of the latex bead) was added to the suspension and incubated for 20 min at r.t. A DTT treatment (f.c. 20 m*M*) was carried out to reduce the PD groups to SH groups. The unreacted DTT and byproducts were separated by GPC, and the NBD-labeled thiol-bearing latex beads [SH-(NBD)latex beads] were collected.

On the other hand, the substrate of the TRITC-labeled rHSA-nanosheets was immersed in a phosphate buffer, and a DMSO solution of EMCS was added to the substrate and incubated for 20 min at r.t. to introduce maleimido groups on the nanosheet. The unreacted EMCS and byproducts were washed with a phosphate buffer, and the maleimido-bearing rHSA-nanosheets were obtained.

Finally, the SH-(NBD)latex beads were added to the maleimido-bearing rHSA-nanosheets, and incubated for 2 h at r.t. The unreacted SH-(NBD)latex beads and byproducts were washed with a phosphate buffer, and the rHSA-nanosheets, of which the obverse side was modified with the NBD-labeled latex beads, were observed using a confocal laser scanning microscope (LSM 510) and a Hitachi S-4500 field emission scanning electron microscope (SEM).

## RESULTS

### Water contact angle

The water contact angle of the substrate, which was coated with ODS-SAM, was estimated to be 83° ± 1° as listed in Table I. When the ODS-SAM-coated substrate was immersed into a phosphate buffer solution (pH 7.4) of rHSA at a concentration of 100 μg/mL, the water contact angle did not change (80° ± 2°). However, when the substrate was immersed in an acetate buffer solution (pH 5.0) of rHSA, the angle was significantly decreased to 67° ± 1°. The angle was restored to 82° ± 1° when the rHSA-treated substrate was immersed into a 1% (v/v) solution of $C_{12}E_{10}$ for 1 h. Therefore, we confirmed

**TABLE I**
**Water Contact Angles of ODS-SAM Before and After rHSA Adsorption**

| rHSA Adsorption | Water Contact Angle (degree) |
|---|---|
| Before | 83 ± 1 |
| After | |
| pH 5.0 | 67 ± 1 |
| pH 7.4 | 80 ± 2 |
| $C_{12}E_{10}$[a] | 82 ± 1 |

[a] $C_{12}E_{10}$ was added to the ODS-SAM after rHSA adsorption at pH 5.0, incubated at r.t. for 1 h and then washed with distilled water.

that rHSA molecules were adsorbed on the ODS-SAM at pH 5.0, and the adsorbed rHSA molecules were detached from the substrate by surfactant treatment.

### Preparation of rHSA-nanosheets

We could not analyze the crosslinking ratio of the SH-rHSA molecules adsorbed on the ODS-SAM from quantification of the unreacted SH groups of the rHSA, because the amount of the adsorbed rHSA was below the detection limit. We explored the crosslinking of the SH-rHSA in an aqueous solution in order to determine the extent of crosslinking of the SH-rHSA on the ODS-SAM. We determined the number of SH groups bound to one rHSA molecule for mixtures of LC-SPDP and rHSA at 5, 7, and 10 mol/mol (mole equivalent of the rHSA concentration) ratios of LC-SPDP to rHSA. Based on the quantification of the 2-TP liberated by the addition of DTT, the number of SH groups bound to one rHSA molecule was estimated to be ~2.9 ± 0.8, 4.7 ± 1.1, and 7.4 ± 1.2 molecules, respectively. We oxidized the SH-rHSA molecules in the presence of copper ion (II) at r.t. and measured the degree of reaction by HPLC with a TSK-GEL G4000SW$_{XL}$ column, by measuring the absorbance of the column effluent at 220 nm, which was attributed to the absorption of the amide linkage of rHSA. At pH 5.0, the three kinds of SH-rHSA having different numbers of SH groups were crosslinked, and the percentage of the peak area of the void fraction to the total peak, which corresponded to the amount of the crosslinked rHSA with a molecular weight of >670 kDa based on the elution time of thyroglobulin as a marker protein, was increased to 64, 75, and 96% with the increasing number of the SH groups bound to one rHSA molecule. All reactions were completed within 12 h. On the other hand, the three kinds of SH-rHSA were hardly crosslinked in the absence of copper ion (II) at pH 5.0 or in the presence of copper ion (II) at pH 7.4. Based on the earlier results, we decided that SH-rHSA molecules with 7.4 ± 1.2 SH groups bound to one rHSA molecule were to be crosslinked on the patterned ODS-SAM at pH 5.0 for 12 h in the presence of 1 $\mu M$ copper ion (II).

Next, we explored the adsorption of SH-rHSA on the rectangle-patterned ODS-SAM regions. When the substrate of the patterned ODS-SAM was immersed in an acetate buffer solution (pH 5.0) of the TRITC-labeled SH-rHSA at a concentration of 1 μg/mL, the rectangular patterns (10 μm × 30 μm) were completely and selectively stained by the TRITC-labeled SH-rHSA as shown in Figure 2(a). After removing the nonadsorbed SH-rHSA by washing with the acetate buffer solution, we crosslinked the SH-rHSA molecules adsorbed on the patterned ODS-SAM following the aforementioned conditions, and immersed the substrate in a 1% $C_{12}E_{10}$ solution at r.t. for 6 h to detach the rectangles from the substrate. Next, we dropped the $C_{12}E_{10}$ solution containing the rectangular sheets onto a glass plate, and observed the surface of the plate using a confocal laser scanning microscopy. There were abundant rectangular rHSA-nanosheets in various conformations; in particular, the bent form of the rHSA-nanosheets was successfully observed in the three-dimensional images [Fig. 2(b,c)], demonstrating the flexible and tough nature of the rHSA-nanosheets.

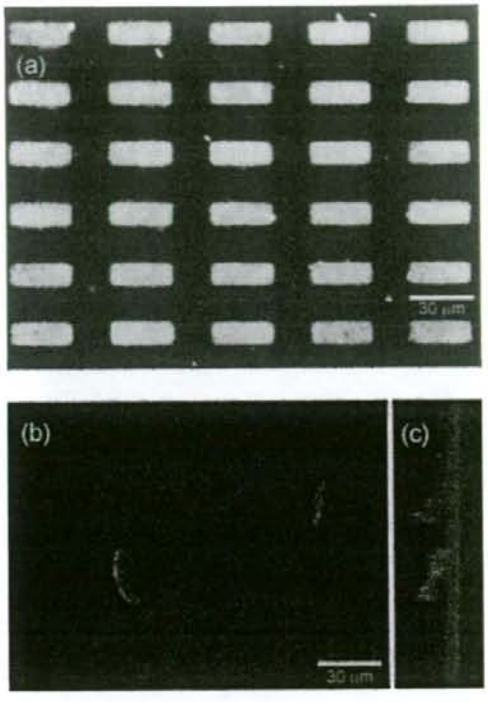


**Figure 2.** (a) Observation of SH-rHSA adsorbed onto the patterned ODS-SAM using fluorescent microscopy. (b) Observation of the free-standing rHSA-nanosheets detached from the patterned ODS-SAM and (c) the 90° rotation image of (b) using confocal laser fluorescent microscopy.

### AFM analysis of rHSA-nanosheets

To establish the morphological detail and the thickness of the rHSA-nanosheets, the nanosheets on the patterned ODS-SAM were observed by AFM. Figure 3(a) shows a large-scale (90 μm × 90 μm), three-dimension AFM image of the rHSA-nano-

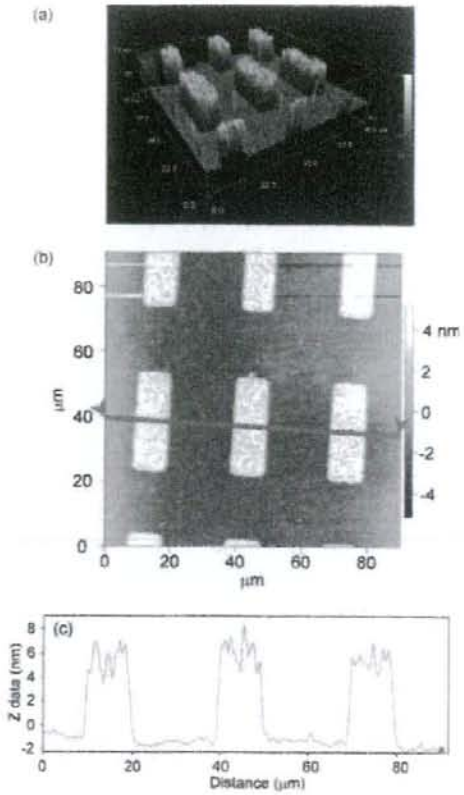


**Figure 3.** AFM images of rHSA-nanosheets adsorbed onto the patterned ODS-SAM. (a) 3-D image, (b) top view image, and (c) cross-sectional image. [Color figure can be viewed in the online issue, which is available at www.interscience.wiley.com.]

sheets. The rectangular patterns (10 μm × 30 μm) were vividly embossed by rHSA, and nonspecific adsorption of rHSA was scarcely observed on the $SiO_2$ regions. From the AFM cross-sectional image, the thickness of the rHSA-nanosheets plus the ODS-SAM was estimated to be 6.6 ± 1.0 nm as shown in Figure 3(b,c). On the other hand, the thickness of the ODS-SAM itself was estimated to be 2.1 ± 0.7 nm (data not shown). Based on the difference between both thicknesses, the thickness of the rHSA-nanosheets was calculated to be 4.5 ± 1.0 nm, which agrees with the dimensions of rHSA.

### rHSA-nanosheets having heterosurfaces

For fabrication of the rHSA-nanosheets having heterosurfaces, we conjugated NBD-labeled latex beads to the obverse side of TRITC-labeled rHSA-nanosheets on ODS-SAM. After the rHSA-nanosheets were detached from the ODS-SAM by the surfactant treatment, the dispersion was put on the cover glass plate, and then the sheets were observed with a confocal laser scanning microscope. There were abundant rectangular rHSA-nanosheets in various conformations (10 μm × 30 μm). We focused on a sheet adopting a bent form as shown in Figure 4. When the rhodamine-labeled rHSA of the sheets was excited at 543 nm, the entire sheet turned red with a measured emission wavelength of over 570 nm as shown in Figure 4(a). On the other hand, NBD of the latex beads was excited at a wavelength of 458 nm and detected in the emission wavelength region from 500 to 530 nm. We observed that the majority of the surface of the sheets turned yellow, and the bent site of the nanosheet was quenched due to the fluorescent resonance energy transfer (FRET) effect from the NBD to the rhodamine as shown in Figure 4(b). When these pictures (a) and (b) were overlayed, the resulting picture (c) clearly showed the red and yellow heterosurfaces, suggesting that NBD-labeled latex beads adhered to the reverse surface at the bent site of the rHSA-nanosheet. Finally, we observed the latex beads-conjugated rHSA-nanosheets on ODS-SAM using an SEM. Many latex beads were specifically conjugated to the obverse side of the rHSA-nanosheets. The contrast of the rHSA-nanosheet was clear and uniform in comparison with that of $SiO_2$ region as shown in Figure 4(e,f), suggesting that the rHSA-nanosheets were thin and flat.

## DISCUSSION

The purpose of this article is to propose a novel method to prepare free-standing biocompatible nanosheets having heterosurfaces, as a new biomaterial, by a combination of four processes as shown in Figure 1: (1) specific adsorption of rHSA molecules onto patterned hydrophobic ODS-SAM regions, (2) preparation of nanosheets of SH-rHSA via two-dimensionally disulfide crosslinking, (3) surface modification of the resulting nanosheets, and (4) preparation of free-standing nanosheets by detachment from the ODS-SAM.

We selected hydrophobic ODS having a terminal $CH_3$ group for the SAM. Wadu-Mestheige et al. reported that bovine serum albumin could be selectively adsorbed on the SAM regions having a terminal $CH_3$ in comparison with SAM regions having a terminal OH or COOH.[26] Since the resulting water contact angle of the ODS-SAM was similar to that of the ODS-SAM in the previous reports,[27,28] we could confirm that the hydrophobic ODS-SAM was certainly constructed on the silicon oxide (Table I).

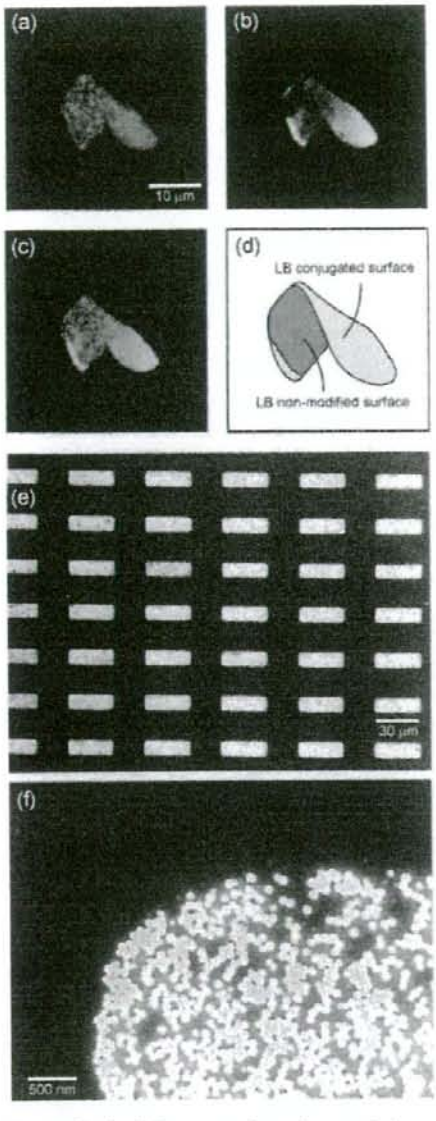


**Figure 4.** Confocal laser scanning microscopic images of rhodamine-labeled rHSA-nanosheets, of which the obverse sides were modified with NBD-labeled latex beads. (a) Rhodamine-conjugated rHSA was excited at a wavelength of 543 nm, and the emission wavelength detected at over 570 nm, (b) NBD conjugated latex beads were excited at a wavelength of 458 nm and the emission wavelength detected at 500–530 nm, (c) the overlayed image of (a) and (b), and (d) Schematic image of rhodamine-labeled rHSA-nanosheets, of which the obverse sides were modified with NBD-labeled latex beads. (e) SEM image of rHSA-nanosheets, of which the obverse sides were modified with latex beads. (f) Magnified SEM image of (e).

As a first step, we investigated the suitable conditions (pH and concentration) for rHSA adsorption onto the ODS-SAM. At pH 7.4, the rHSA molecules did not adsorb on the ODS-SAM, as seen from the contact angle measurement (Table I). At that pH, the charge of rHSA is negative, because the isoelectric point of rHSA is 4.9. Above that pH, rHSA molecules have little hydrophobic interaction with ODS-SAM and repel each other electrostatically. Therefore, they favor remaining dissociated in the solution rather than to assemble onto the ODS-SAM, resulting in no change in the contact angle. At pH 5.0, near the isoelectric point of rHSA, the contact angle was significantly decreased, suggesting that the rHSA molecules were firmly adsorbed on the ODS-SAM. As described later in the final step, the water contact angle after the surfactant treatment was comparable to that of the ODS-SAM before rHSA adsorption, indicating that the attractive force giving rise to the adsorption of rHSA on the ODS-SAM was hydrophobic interaction. These results are consistent with the previous reported experiments on albumin adsorption at pH 5.0 and influences the three-dimensional shape of the individual albumin adsorbed on the terminal $CH_3$ of SAM.[29,30] These previous studies reported on the adsorption mechanism of albumin onto the SAM as the following: the electrostatic repulsion among albumin molecules was decreased at pH 5.0 and the interprotein interaction (mostly hydrophobic interaction) strengthened, thus the albumin immobilized on the SAM was more stable than individual proteins in the solution state.

Next, at pH 5.0 and r.t., we explored the optimum concentration of the TRITC-labeled SH-rHSA adsorbed on the patterned ODS-SAM. In the case of the TRITC-labeled SH-rHSA at a concentration of 10 μg/mL or over, the rectangular patterns were distinctly stained by fluorescence; however, the SH-rHSA molecules were nonspecifically adsorbed on the hydrophilic silicon oxide regions and brightened the background (data not shown). In the case of the SH-rHSA at a concentration of 0.1 μg/mL, the ODS patterns were hardly stained (data not shown). At a concentration of 1 μg/mL, almost all the ODS patterns were selectively stained (Fig. 2) and the rHSA molecules were predominantly located in the patterned ODS region (Fig. 3). The number of the ODS patterns arranged on the substrate (1 cm × 1 cm) is estimated to be $\sim 6.7 \times 10^4$, and the number of rHSA molecules adsorbed on one patterned ODS region was calculated to be $\sim 1.2 \times 10^7$ molecules, if the average surface area of one rHSA molecule is 25.5 $nm^2$,[31] and rHSA molecules are closely packed in the patterned ODS region (rectangular patterns: 10 μm × 30 μm, area: $3.0 \times 10^8$ $nm^2$). Accordingly, the total number of the rHSA molecules adsorbing on the ODS patterns was calculated to be $\sim 8.0 \times 10^{11}$ mole-

cules. Approximately 9% of the total rHSA was estimated to be adsorbed onto the ODS regions by immersing the substrate in the 1 mL rHSA solution at a concentration of 1 μg/mL, containing $9.0 \times 10^{12}$ rHSA molecules. This was also supported by the results obtained from the other patterns such as circles and squares (data not shown). Consequently, we set the conditions of the rHSA adsorption onto the patterned ODS-SAM, at pH 5.0, at r.t. and the concentration of 1 μg/mL.

The second step of the process is to crosslink each SH-rHSA molecule adsorbed on the patterned ODS-SAM to prepare nanosheets. We presumed that once the SH-rHSA molecules were adsorbed onto the substrate they would closely pack in the pattern, and thus be easy to crosslink in comparison with those in an aqueous solution. We utilized the crosslinking conditions for SH-rHSA in an aqueous solution to estimate the necessary conditions for crosslinking on the ODS-SAM. Crosslinking of the SH-rHSA by *N*-succinimidyl 3-(2-pyridyldithio) propionate (SPDP, spacer length is 0.68 nm), which has a terminal succinimidyl group and a pyridyldisulfide group to introduce the SH group to the surface of rHSA molecule after a DTT treatment, failed probably because the spacer length of SPDP would be too short to crosslink. Referring to a report by Komatsu et al., where a dimer and clusters of rHSA had been exquisitely synthesized using a bis-maleimidohexane and an LC-SPDP, which have spacer lengths of 1.61 and 1.57 nm, respectively,[31,32] we used the LC-SPDP, which has similar functionality as that of SPDP. Only a small proportion of the SH-rHSA molecules crosslink at pH 7.4 in the presence of copper ion (II) as described in a previous report,[25] suggesting that the rHSA molecules electrostatically repel each other because of the negative ζ-potential of the rHSA molecule. At pH 5.0, near the isoelectric point (p*I* = 4.9), the SH-rHSA was significantly crosslinked. The percentage of the peak areas of the void fractions for the total peak areas, which corresponded to the amount of the crosslinked rHSA over the molecular weight of 670 kDa, increased with the increasing number of the SH groups bound to one rHSA molecule. On the other hand, the crosslinking of the SH-rHSA was extremely slow in the absence of copper ion (II). The thiol oxidation is commonly facilitated in alkaline conditions because of complexation of copper ion (II) with thiolate anions.[25] However, we used the weakly acidic conditions (pH 5.0), where the reaction rate was considered to be slow, suggesting that the thiol oxidation of the rHSA molecules would be controlled by electrostatic repulsion and hydrophobic interaction of rHSA molecules. Based on the earlier results, we could crosslink the SH-rHSA molecules adsorbed on the patterned ODS-SAM at pH 5.0 in the presence of 1 μ*M* copper ion (II).

We measured the thickness of the rHSA-nanosheets as 4.5 ± 1.0 nm from the thickness of the ODS-SAM alone and the rHSA-nanosheet adsorbed on the ODS-SAM using AFM (Fig. 3). Carter and Ho reported that the tertiary structure of the HSA molecule determined from X-ray diffractometry could be described as a heart-shaped or equilateral triangular molecule, with each side 8 nm in length and with an average thickness of 3 nm.[33] The result showed that the rHSA-nanosheets could be regarded as a monolayer of SH-rHSA. As the hydrophobic interaction of SH-rHSA molecules with ODS-SAM should be stronger than that of SH-rHSA molecules with each other, the rHSA molecules weakly adsorbed onto the rHSA monolayer could be removed by washing before the addition of copper ion (II) as a catalyst of disulfide crosslinking. Furthermore, we confirmed that the nonspecific adsorption onto the $SiO_2$ surface was extremely reduced if the substrate were immersed into the rHSA solution under the aforementioned conditions, based on the results obtained by AFM as well as fluorescent microscopy.

In the third step, we tried to modify the surface of the resulting nanosheet with latex beads, which were useful carriers because of their uniform size and ease of confirmation by microscopic observation. We conjugated the NBD-labeled latex beads onto the obverse side of the TRITC-labeled rHSA-nanosheets that had been adsorbed on the ODS-SAM and demonstrated the preparation of nanosheets having heterosurfaces. As shown in Figure 4, there were many rHSA-nanosheets in various conformations of rectangles, such as bent forms. Surprisingly, there were no broken sheets, suggesting that the rHSA-nanosheets are tough and extremely flexible. Focusing on the nanosheet having a bent form (Fig. 4), when the rhodamine-labeled sheets were excited at 543 nm, the entire sheet turned red with a measured emission wavelength of over 570 nm [Fig. 4(a)]. On the other hand, we tried to detect the NBD on the surface of the sheet as yellow at the excitation of 458 nm and at the emission wavelength region from 500 to 530 nm. We could observe that the obverse surface of the sheet was colored yellow, and the reverse side (bent site) was significantly quenched [Fig. 4(b)]. Since the FRET efficiency is related to the inverse six power of the distance between the acceptor and donor probes, the technique is elegantly used to measure the molecular distance at the 1.5–7.5 nm range.[34,35] Based on the earlier information and judging from the thickness of the rHSA-nanosheet, the quenching of the NBD emission from the bent side of the nanosheet was caused by the FRET effect from NBD to rhodamine. It also indicates that the NBD-latex beads are attached only to the obverse side of the nanosheet. If a sufficient amount of the NBD-latex beads were attached to both sides of the

sheet, then both sides of the sheet would be quenched. Furthermore, we also confirmed that the latex beads were specifically conjugated to the obverse side of the rHSA-nanosheets using an SEM [Fig. 4(e,f)]. The nanosheets released from the substrate after conjugating the latex beads were heterogeneously modified.

In the final step, we investigated a method to detach the rHSA-nanosheets from the patterned ODS-SAM. We selected $C_{12}E_{10}$ as a nonionic surfactant for which surfactant ability was independent of pH change. As shown in Table I, when the substrate, to which rHSA (non-SH modification) molecules were adsorbed, was immersed into a 1% (v/v) solution of $C_{12}E_{10}$ for 1 h at r.t., the water contact angle was returned to that of the ODS-SAM before rHSA adsorption. This indicated that the rHSA adsorbed on the ODS-SAM was detached by the addition of a $C_{12}E_{10}$, and the attractive force giving rise to the adsorption of rHSA on the ODS-SAM was hydrophobic interaction. In the first and second processes, the SH-rHSA molecules were selectively adsorbed onto the patterned ODS regions and crosslinked in the presence of copper ion (II) to prepare the rHSA-nanosheets. Very few of the resulting nanosheets were detached from the substrate by immersion in the 1% $C_{12}E_{10}$ solution for 1 h, whereas the control rHSA could simply detach. It took at least 6 h to detach the nanosheet from the substrate with the 1% $C_{12}E_{10}$ solution. On the other hand, we also conformed that the nanosheets were completely dissolved after 1 h by a DTT treatment (data not shown). This suggested that it was difficult for the $C_{12}E_{10}$ molecules to diffuse into the spaces between the nanosheets and the ODS-SAM substrate, because the nanosheet was composed of sufficiently two-dimensionally crosslinked rHSA by intermolecular oxidation of thiol groups. Furthermore, we confirmed that the resulting rHSA-nanosheets were stable in the presence of $C_{12}E_{10}$, because the sheet shapes did not change after the $C_{12}E_{10}$ removal by dialysis (data not shown).

Using a confocal laser scanning microscopy, we fortunately observed the rHSA-nanosheets in three-dimensional images and confirmed them to be a curved form [Fig. 2(c), and figure of supporting information]. On the basis of analyses of quartz crystal microbalance and grazing angle infrared spectroscopy, Roach et al. reported that albumin had enough adsorption affinity toward the hydrophobic ($CH_3$ terminus) compared to the hydrophilic surface (OH terminus), to cause adsorption-induced deformation.[36] Furthermore, Zeng et al. showed through modeling that the orientation of the adsorbed protein (lysozyme) was dependent on the discrete organization of the functional groups presented on the SAM surface, and in the case of the hydrophobic $CH_3$ group, hydrophobic amino residues of the protein were closest to the surface.[37] From these references, we suggested that the rHSA-nanosheets would adopt a curved form, because the wettability of the obverse and reverse surface of the rHSA-nanosheets was different, that is, the obverse surface appeared to be more hydrophilic than the reverse surface. Consequently, we succeeded in the detachment of the rHSA-nanosheets from the ODS-SAM by mild conditions such as surfactant immersion in order to obtain uniform rHSA-nanosheets.

## CONCLUSIONS

We succeeded in the preparation of free-standing rectangular (10 × 30 μm) and ultrathin (4.5 ± 1.0 nm) rHSA-nanosheets by two-dimensional crosslinking via disulfide bonds on a patterned ODS-SAM, and could also obtain free-standing rHSA-nanosheets having heterosurfaces by surface modification with fluorescent latex beads. Thus, the rHSA-nanosheets may be a suitable candidate as a new biomaterial for drug-delivery carriers, hemostatic reagents, wound dressing for burn injury, and so forth. In our future work, we are preparing the rHSA-nanosheets on a large scale to carry the recombinant fragments of platelet membrane protein and/or dodecapeptides such as GPIbα and H12 to evaluate their performance *in vitro* and *in vivo*.

Y.O. was the recipient of a Research Fellowships from the JSPS for Young Scientists and the recipient of Japan Health Sciences Foundation.

## References

1. Tomii Y. Lipid formation as a drug carrier for drug delivery. Cur Pharma Design 2002;8:467–474.
2. Takeoka S, Teramura Y, Okamura Y, Handa M, Ikeda Y, Tsuchida E. Fibrinogen-conjugated albumin polymers and their interaction with platelets under flow conditions. Biomacromolecules 2001;2:1192–1197.
3. Takeoka S, Teramura Y, Ohkawa H, Ikeda Y, Tsuchida E. Conjugation of von Willebrand factor-binding domain of platelet glycoprotein Ibα to size-controlled albumin microspheres. Biomacromolecules 2000;1:290–295.
4. Teramura Y, Okamura Y, Takeoka S, Tsuchiyama H, Narumi H, Kainoh M, Handa M, Ikeda Y, Tsuchida E. Hemostatic effects of polymerized albumin particles bearing rGPIa/IIa in thrombocytopenic mice. Biochem Biophys Res Commun 2003; 306:256–260.
5. Okamura Y, Takeoka S, Teramura Y, Maruyama Y, Tsuchida E, Handa M, Ikeda Y. Hemostatic effects of fibrinogen-γ chain dodecapeptide-conjugated polymerized albumin particles *in vitro* and *in vivo*. Transfusion 2005;45:1221–1228.
6. Takeoka S, Teramura Y, Okamura Y, Tsuchida E, Handa M, Ikeda Y. Rolling properties of rGPIbα-conjugated phospholipid vesicles with different membrane flexibilities on vWf surface under flow conditions. Biochem Biophys Res Commun 2002;296:765–770.

7. Okamura Y, Maekawa I, Teramura Y, Maruyama Y, Tsuchida E, Handa M, Ikeda Y, Takeoka S. Hemostatic effects of phospholipid vesicles carrying fibrinogen-γ chain dodecapeptide *in vitro* and *in vivo*. Bioconjug Chem 2005;16:1589–1596.
8. Okamura Y, Handa M, Suzuki H, Ikeda Y, Takeoka S. New strategy of platelet substitutes for enhancing platelet aggregation at high shear rates; cooperative effects of a mixed system of fibrinogen γ-chain dodecapeptide- or glycoprotein Ibα-conjugated latex beads under flow conditions. J Artif Organs 2006;9:251–258.
9. Takeoka S, Okamura Y, Teramura Y, Watanabe N, Suzuki H, Tsuchida E, Handa M, Ikeda Y. Function of fibrinogen γ-chain dodecapeptide-conjugated latex beads under flow. Biochem Biophys Res Commun 2003;312:773–779.
10. Mattson J, Forrest JA, Borjesson L. Quantifying glass transition behaviour in ultrathin free-standing polymer films. Phys Rev E 2000;62:5187–5200.
11. Tang Z, Kotov NA, Magonov S, Ozturk B. Nanostructured artificial nacre. Nat Mater 2003;2:413–418.
12. Mallwitz F, Laschewsky A. Direct access to stable, freestanding polymer membranes by layer-by-layer assembly of polyelectrolytes. Adv Mater 2005;17:1296–1299.
13. Mamedov A, Kotov NA, Prato M, Guldi DM, Wicksted JP, Hirsch A. Molecular design of strong single-wall carbon nanotube/polyelectrolyte multiplayer composites. Nature Mater 2002;1:190–194.
14. Huck WT, Stroock AD, Whitesides GM. Synthesis of geometrically well-defined, molecularly thin polymer films. Angew Chem Int Ed 2000;39:1058–1061.
15. Mamedov A, Kotov N. Free-standing layer-by-layer assembled films of magnetite nanoparticles. Langmuir 2000;16:5530–5533.
16. Mallwitz F, Goedel WA. Physically cross-linked ultrathin elastomeric membranes. Angew Chem Int Ed 2001;40:2645–2647.
17. Eck W, Küller A, Grunze M, Völkel B, Gölzhäuser A. Freestanding nanosheets from crosslinked biphenyl self-assembled monolayers. Adv Mater 2005;17:2583–2587.
18. Xu H, Goedel WA. Polymer-silica hybrid monolayers as precursors for ultrathin free-standing porous membranes. Langumuir 2002;18:2363–2367.
19. Nardin C, Winterhalter M, Meier W. Giant free-standing ABA triblock copolymer membranes. Langmuir 2000;16:7708–7712.
20. Ulman A. An Introduction to Ultrathin Organic Films from Langmuir–Blodgett to Self-Assembly. San Diego, CA: Academic Press; 1991.
21. Khoshtariya DE, Wei J, Liu H, Yue H, Waldeck DH. Charge-transfer mechanism for cytochrome c adsorbed on nanometer thick films. Distinguishing frictional control from conformational gating. J Am Chem Soc 2003;125:7704–7714.
22. Ferapontova EE, Shipovskov S, Gorton L. Bioelectrocatalytic detection of theophylline at theophylline oxidase electrodes. Biosens Bioelectron 2007;22:2508–2515.
23. Niwa D, Yamada Y, Homma T, Osaka T. Formation of molecular templates for fabricating on-chip biosensing devices. J Phys Chem B 2004;108:3240–3245.
24. Sugimura H, Ushiyama H, Hozumi A, Takai O. Micropatterning of alkyl- and fluoroalkylsilane self-assembled monolayers using vacuum ultraviolet light. Langmuir 2000;16:885–888.
25. Cavallini D, De Marco C, Dupre S, Rotilio G. The copper-catalyzed oxidation of cysteine to cystine. Arch Biochem Biophys 1969;130:354–361.
26. Wadu-Mestherige K, Amro NA, Liu GU. Immobilization of proteins on self-assembled monolayers. Scanning 2000;22:380–288.
27. Siqueira PDF, Wenz G, Schunk P, Schimmel T. An improved method for the assembly of amino-terminated monolayers on $SiO_2$ and the vapor deposition of gold layers. Langmuir 1999;15:4520–4523.
28. Depalma V, Tillman N. Friction and wear of self-assembled trichlorosilane monolayer films on silicon. Langmuir 1989;5:868–872.
29. Norde W, Giesbers M, Pingsheng H. Langmuir–Blodgett films of polymerized 10,12-pentacosadiyonic acid as substrates for protein adsorption. Colloids Surf B 1995;5:255–263.
30. Prime KL, Whitesides GM. Adsorption of proteins onto surfaces containing end-attached oligo(ethylene oxide): A model system using self-assembled monolayers. J Am Chem Soc 1993;115:10714–10721.
31. Komatsu T, Oguro Y, Teramura Y, Takeoka S, Okai J, Anraku M, Otagiri M, Tsuchida E. Physicochemical characterization of cross-linked human serum albumin dimer and its synthetic heme hybrid as an oxygen carrier. Biochim Biophys Acta 2004;1675:21–31.
32. Komatsu T, Oguro Y, Nakagawa A, Tsuchida E. Albumin clusters: Structurally defined protein tetramer and oxygen carrier including thirty-two iron(II) porphyrins. Biomacromolecules 2005;6:3397–3403.
33. Carter DC, Ho JX. Structure of serum albumin. Adv Protein Chem 1994;45:153–204.
34. Stryer L, Haugland RP. Energy transfer: A spectroscopic ruler. Proc Natl Acad Sci USA 1967;58:719–726.
35. Stryer L. Fluorescence energy transfer as a spectroscopic ruler. Ann Rev Biochem 1978;47:819–946.
36. Roach P, Farrar D, Perry CC. Interpretation of protein adsorption: Surface-induced conformational changes. J Am Chem Soc 2005;127:8168–8173.
37. Zeng J, Li L, Chen S, Jiang S. Molecular simulation study of water interactions with oligo (ethylene glycol)-terminated alkanethiol self-assembled monolayers. Langmuir 2004;20:8931–8938.